Mechanism to Quantify Road Surface Degradation and Its Impact on Rolling Resistance

Thesis

Presented in Partial Fulfillment of the Requirements for the Degree Master of Science in the Graduate School of The Ohio State University

By

Dina Caicedo Parra, B.S.

Graduate Program in Mechanical Engineering

The Ohio State University

2019

Thesis Committee

Prof. Giorgio Rizzoni, Advisor

Prof. Mei Zhuang

Dr. Adithya Jayakumar

Abstract

To measure the exact fuel consumption of a vehicle, it is essential to determine the total road load being imparted on it. One of the main methods to calculate road load is by performing a coast-down test. In order to get accurate results, there must be an understanding of the impact that each component has on the vehicle/tire. Rolling resistance is one of the primary forces acting against the motion of the vehicle. The major factors that contribute to rolling resistance losses are tire design and operation, ambient conditions and road design. Current standards tend to assume that the impact of a specific road surface in a coast-down test is a constant parameter. However, after performing multiple coast-down tests in the same track, this will cause the road surface texture to degrade. Even with a small degradation, this will possibly affect the results since the rolling resistance coefficient is increasing as well as the road load affecting the vehicle.

This thesis provides a framework for road surface degradation due to coast-down testing during a span of one and a half years. First, an overview of road surface texture and its impact on fuel consumption is introduced. Surface texture is composed by 4 wavelengths, each one affecting in different ways the vehicle/tire interaction. This thesis focuses on the two smallest wavelengths -macrotexture and microtexture. Advantages and disadvantages of different methods for measuring road surface are discussed. Then, experimental data was collected with an optical profilometer in a coast-down track before and after it was

repaved. This thesis aims to quantify the degradation that each wavelength experienced and to analyze the data as thorough as possible. Also, additional measurements were collected to study the impact of weather effect in the long run. By assuming a linear degradation, a mathematical model is developed to estimate the surface texture value. With more tight fuel consumption and emission regulations, it is important for automakers to account or model the change in surface texture that impacts coast-down tests and potentially would also impact fuel consumption.

Dedication

This thesis is dedicated to the one person who has always supported me and without her I wouldn't be here today, always grateful for the unconditional love of my mom.

Acknowledgments

There are many people that I would like to thank and who were a positive impact throughout my Ohio State experience. First, I am enormously grateful for the opportunity that Professor Rizzoni gave me. His mentoring and support were fundamental to be able to accomplish this work. Also, I would like to thank Dr. Jayakumar for allowing me to participate in this project, it's been an incredible experience from which I have obtained valuable knowledge. Thanks to all the students and staff at the Center for Automotive Research.

Vita

Summer 2014……..…. Project Engineer Intern, CCC, Des Moines, IA

Summer 2015……Purdue University research assistant, West Lafayette, IN

Summer 2016……Engine optimization Intern, Cummins, Columbus, IN

December 2016…….B.S. Aerospace Engineering, Iowa State University, Ames, IA

January- August 2017…….....Engine optimization, Intern, Cummins, Columbus, IN

Summer 2018……...Powertrain Integration Intern, Cummins, Columbus, IN

2017-Present……Graduate Research Assistant, Department of Mechanical Engineering, The Ohio State University

Publications

Ramesh, A., Shaver, G., Allen, C., Caicedo Parra, D., et al. "Utilizing low airflow strategies, including cylinder deactivation, to improve fuel efficiency and aftertreatment thermal management". International Journal of Engine Research, 2017

Fields of Study

Major Field: Mechanical Engineering

Table of Contents

List of Tables

List of Figures

Chapter 1 : Introduction

1.1 Overview:

With the increase in demand in vehicles but also more strict emission regulations, automakers are trying to improve the fuel economy of their vehicles by different approaches. The estimation of fuel economy is done in a laboratory by simulating real drive conditions as close as possible. However, multiple customers have complained about automakers, affirming that the fuel efficiency of their cars does not match the advertised claims. Companies are trying to improve their procedures for calculating the fuel economy of their vehicles in order to obtain more accurate numbers.

This thesis develops a methodology for an improved estimation of vehicle road load that is used to estimate a vehicle's fuel economy. The main focus of this thesis is how road degradation makes an impact in the calculation of the road load. Road surface texture is a parameter that most automakers assume is constant between the time of repaving and the next one (there could be years in-between). Throughout this work, a new model describing the surface texture is developed. This model is stablished based on experimental data collected from a proving ground, and by analyzing the different wavelengths that affect surface texture. This model plays an important factor for trying to characterize the road load affecting a vehicle.

1.2 Motivation:

Mainly based on the oil embargo of 1973, Congress decided to establish the CAFE standards in the mid-1970s. These standards had the intention of setting an average vehicle fuel economy that manufacturer's fleet must achieve depending on the type of vehicle. Then, under the Energy Policy and Conservation Act all new light duty cars and trucks were required to display fuel economy labels on the window sticker [1]. The new regulations quickly started to show results, and a 2002 study made by the National Academy of Sciences concluded that motor vehicle fuel usage had reduced 14 percent compared to what it would have been in the absence of fuel efficiency standards [2]. Throughout the years, the required fuel economy has been updated many times to account for improved vehicle testing, new vehicle technologies, driving conditions, new regulations, etc.

In 2009 The National Program was established as an agreement between the federal government, state regulators, and the auto industry to implement the first meaningful fuel efficiency developments (in over 30 years) and the first greenhouse gas emissions standards for light-duty vehicles [3] [4]. At first, the standards were established in a one-phase program for vehicles model year 2012-2016.

In 2012 Obama's administration extended the National Program to have a second phase for vehicles model year 2017-2025. Additionally, there was a modification to the CAFE regulations to require further improvements in fuel economy. The new regulations aim to reach an average fleet fuel economy of 54.5 miles per gallon by 2025 [5]. Larger vehicle

(light trucks) and a small passenger car would be subject to different requirements due to different vehicle footprints. These demands have increased pressure on vehicle manufacturers to improve their products by reducing fuel consumption and exhaust emissions.

In the last years, federal laws requiring an increase in fuel economy have become a necessity mainly due to the doubling of annual vehicle miles traveled, and an increase in the market share of less efficient SUVs and light trucks [4]. Around 40 percent of the nearly new vehicles that will come off lease in 2018 in US will be SUVs and crossrovers, and there are predictions that this percent will increase in the following years [6].

In order to reach a higher fuel economy, companies are innovating and applying new technologies in the entire vehicle system. Some of the most common implementations are to include hybrid-electric powertrains, 9- and 10-speed transmissions, direct injection and/or turbocharging [7]. In the last couple of years, there has been an elevated amount of investment in the area of electrification and batteries to incorporate in vehicles to make them cleaner and with a better performance. Several governments are encouraging companies to develop more electrification related technologies with various incentives [8] [9] [10] .

Figure (1.1) represents the current and expected passenger car miles per gallon for various countries (primarily due to the different regulations in each country). Between 2000 and 2025, fuel economy in US is expected to almost double. It is important to note how the miles per gallon are projected to significantly keep increasing due to the expectation of new technology being developed. In addition, this increase is also complemented by a higher power output, lower 0-60 mph times and more advance safety technologies.

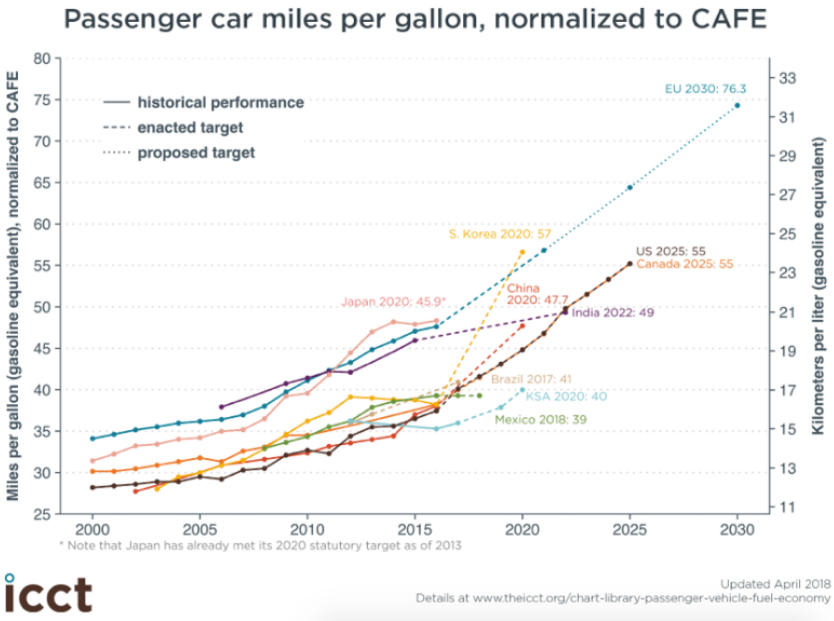

Figure 1-1 Miles per gallon [65]

Regulations for higher fuel economy not only saves consumers money at the pump, but it also creates new jobs, develops innovative technologies, and cuts global warming pollution. Since the year when the Obama administration increased the CAFÉ standards, jobs in automotive components manufacturing have risen by nearly 30% [11]. Automakers have departments dedicated only to study vehicle's fuel consumption, what parameters affect it in a positive or negative way and how to improve it. These studies motivate companies to question the way a component or method has always worked and how to design it in a better way. Fuel efficiency standards are an important driver of performance, innovation and progress.

1.3 Scope:

Primarily, fuel economy is measured under controlled conditions in a laboratory using a series of specific driving cycles dictated by federal law. These driving cycles allow a quantitative assessment of fuel consumption and greenhouse gases. Different countries have developed their own driving cycles, which are represented as traces of vehicle speed versus time. In US, there are two main models that are used to represent the most common driving conditions. Figure (1.2) shows the FTP-75, which is a transient test for passenger cars and light duty trucks that simulates an urban route with frequent stops. This test is divided in 3 phases – cold start, stabilized phase and hot start phase. For the hot start phase, the vehicle is stopped for 10 minutes right after the stabilized phase and then started. Figure (1.3) represents the HWFET (highway fuel economy test), which is designed for light duty vehicles and replicates highway conditions. There are other drive cycle tests designed to simulate aggressive driving behavior, influence of air conditioning, low speed city driving, etc.

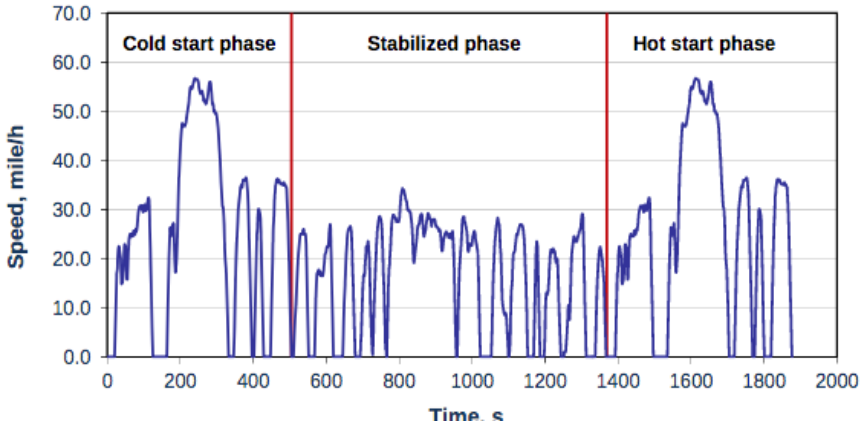

Figure 1-2 FTP-75 [66]

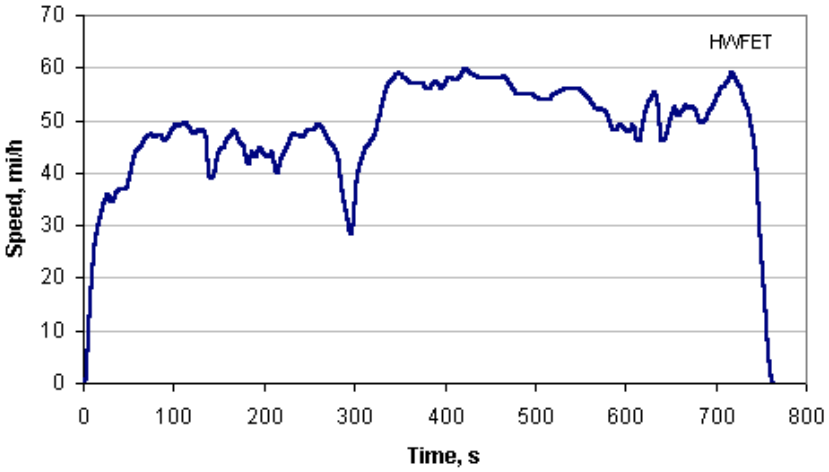

Figure 1-3 HWFET [66]

For evaluating the drive cycles, the vehicle is tested on a chassis dynamometer where the load at the wheel is adjusted to match the road load conditions. The site where the dynamometer is located should be in a controlled thermal state, where both temperature and humidity are controlled. A simplified model is used to impose load on the vehicle under test. The model in question consists of an approximation of road load or power required to motor a vehicle. Road load is composed mainly of 4 components; figure (1.4) represents each force: aerodynamic drag, rolling resistance from tires, grade and inertial loads (accelerating the vehicle) [12].

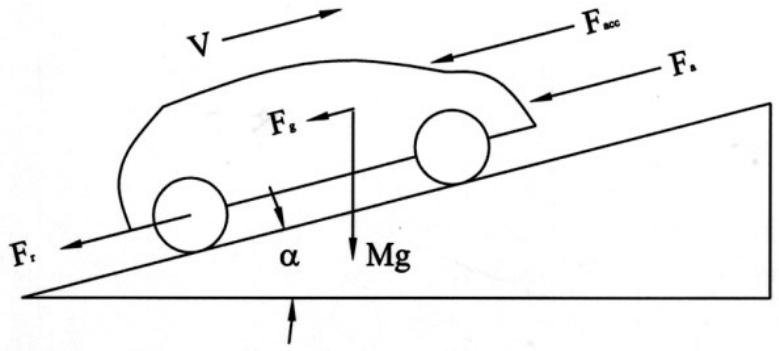

Figure 1-4 Road load components in a vehicle [12]

The road load would be the sum of the forces against the vehicle motion:

$$F_{road\ load}(t) = F_a(t) + F_g(t) + F_r(t) + F_{acc}(t) \qquad (1.1)$$

The following equations represent each parameter:

$$F_{aero} = \frac{1}{2} C_d A_f \rho_a V_{eff}^2 \qquad (1.2)$$

$$F_{RR} = Mgcos(\alpha) C_r(v) \qquad (1.3)$$

$$F_g = Mgsin(\alpha) \qquad (1.4)$$

F_{acc} : Usually a percentage value is assumed

As a result,

$$F_{road\ load} = \frac{1}{2} C_d A_f \rho_a V_{eff}^2 + Mgsin(\alpha) + Mgcos(\alpha) C_r + F_{acc} \qquad (1.5)$$

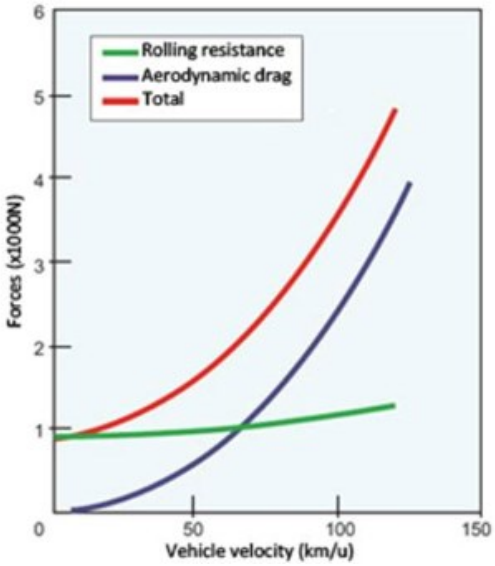

Figure 1-5 Forces on vehicle [13]

Figure (1.5) represents the main forces acting on a vehicle (assuming grade=0). It is observed how each force has a different impact on fuel consumption at each speed. Also, this will vary from vehicle to vehicle; for example, the aerodynamic drag would have a greater impact on a truck compared to a passenger car. For an exact value on fuel consumption, each of the road load parameters would need to be measure, and then input into the dynamometer.

The Environmental Protection Agency (EPA) established that a Coast Down test should be performed in order to characterize the road load force acting on a vehicle. Coast-down test is a common method in industry that captures real driving conditions and parameters acting on a car. In general, during a coast-down test the vehicle is equipped with an anemometer to record air velocity (speed and direction) and a device to record time and vehicle speed.

At first a vehicle is driven for a minimum of 30 minutes at 50mph to precondition the vehicle and tires. Then, the vehicle accelerates to an approximate speed of 80 mph, which is 10mph above the highest speed in the coast-down range. After stabilizing in the required speed, the transmission is shifted into neutral and the data loggers are turned on to collect vehicle speed and time data. The vehicle freely coasts until it reaches a speed below 9 mph. A minimum of 10 runs are made in alternating directions due to wind effects and averaged at the end.

It is important to notice that there are certain required ambient conditions necessary for doing a coast-down:

- Ambient temperature should be between 5 and 35C (41 to 95F)
- The road shall be level and the slope shall be constant within ± %1.0 and not exceed 1.5%.
- Road tests shall be performed on a road or test track and the roads shall be dry, clean, and smooth.
- Average cross winds should not exceed 15 km/h (9.3 mi/h)

For the complete list of requirements please refer to [14].

The reduction in velocity is linked to the friction resistance losses that the vehicle experiences. The experimental data collected is used to fit the coefficients of the following model:

$$F_{road\ load}(v) = A + Bv + Cv^2 \qquad (1.6)$$

A, B and C are referred to as the coast-down coefficients, and they are used for running the various drive cycles. Automakers ensure that there is not any double counting of loads due to the loads on the dynamometer.

While a coast-down is in principle capable of capturing all the major components of the vehicle road load, in fact this test has many uncertainties that have to do with among other environmental conditions (temperature, pressure, altitude, etc.) and the nature of the road surface (texture, roughness, etc.). These uncertainties could be part of the reason why in some cases the fuel economy label does not match completely with real driving scenarios. There have been discrepancies between these two values throughout different companies [15] [16].

The current methodology in US for doing a coast-down test was proposed by the Society of Automotive Engineers (SAE) in 1996 and was updated in 2008 based on new studies [14]. Even though SAE recommends a methodology there is a certain flexibility allowed in the manufacturer's road load test procedures. As a result, automakers perform the coast-down test with certain differences that could lead to variations in the final result.

1.4 Objectives and organization of thesis

The main objective of this thesis is to do a deep analysis on what parameters affect rolling resistance with a focus on the effect of surface texture. This analysis is done with experimental data and its results contribute to a better characterization of rolling resistance which is necessary for accurate results when calculating fuel consumption.

Following the introduction, this thesis is organized in 5 chapters. A brief description of the contents of each chapter is as follows:

- Chapter 2: This chapter goes over a general overview and background of different methods to assess fuel economy and how vehicle losses are measure. An emphasis is placed on the parameters that affect rolling resistance in tires, especially on road surface texture. Through different sources it is shown how road surface greatly impacts fuel consumption and ride quality.
- Chapter 3: A comparison between different devices to measure road surface is discussed. Then, the accuracy and resolution of a profilometer is explained to have a better understanding of the data. The methodology for measuring road surface degradation depending on its wavelength is presented.
- Chapter 4: The approach to process the raw data is explained. Then, results of road surface degradation for different wavelengths is shown. This chapter deals with the data analysis to understand what the results represent and how accurate they are. A linear model is used to determine a road degradation model.
- Chapter 5: Finally, this chapter gives a summary of the conclusions drawn from the previous chapters and how this work could be implemented in future studies.

Chapter 2 : Literature Review and Background

As discussed in chapter 1, coast-down is a universal procedure for measuring all the forces acting on a vehicle while driving over a smooth level surface. This process is done for different reasons, but mainly it is to obtain valuable information about vehicle performance and its interaction with the environment.

One of the major problems in road load data analysis is developing an accurate mathematical model of F_{aero}, F_{RR} and $F_{driveline}$ to accurately obtain the same result for each parameter on the track and in a wind tunnel. This chapter gives an overview of what elements affect each parameter and how they have been modeled with an emphasis in rolling resistance.

2.1 Aerodynamic drag force

In a coast-down test, aerodynamic drag is the main influencer on a vehicle's fuel consumption, especially at higher speeds (above 45 km/h). Aerodynamic drag force can be estimated in two ways, one is by doing a coast-down on a road and the other one in an aerodynamic wind tunnel.

A coast-down test estimates the aerodynamic drag force by measuring how the vehicle decelerates from a specific initial speed when the tractive power is 0 (transmission is

disengaged). The rate of vehicle deceleration, the velocity profile, is an indicator of all the drag forces acting on the vehicle. To collect data with respect to the aerodynamic drag effect, an anemometer is placed in a vehicle to continuously record the wind speed and speed direction. SAE J2263 suggests using a boom-mounted anemometer approximately 2m in front of the vehicle, as represented in figure (2.1) [14].

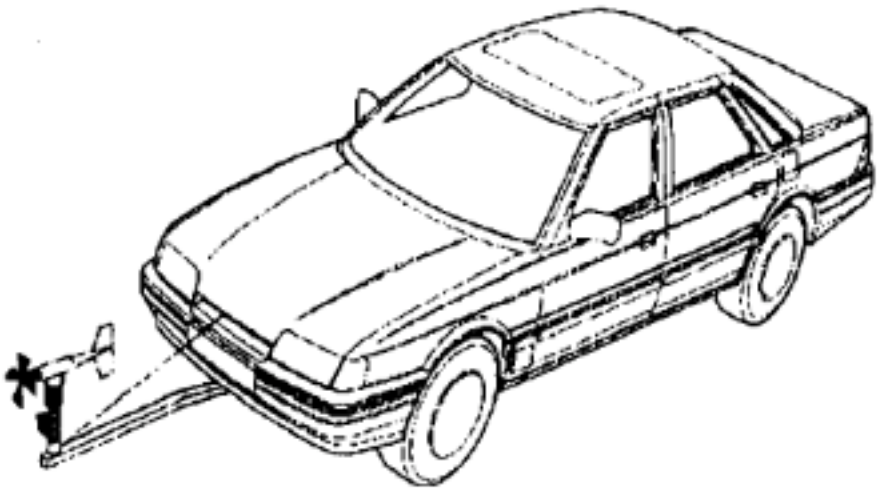

Figure 2-1 Vehicle with anemometer

Then, for isolating the aerodynamic drag force, one can perform a wind tunnel test with the same vehicle set-up as in the coast-down. To characterize the aerodynamic forces in a wind tunnel, it is important to represent the actual air flow around the vehicles as accurately as possible, because the forces and moments represent an integration of the pressure field over the vehicle. Since pressure is proportional to velocity squared, small errors could cause significant discrepancies.

As previously defined, aerodynamic drag is generally represented by equation (1.2). However, if the ambient wind data includes crosswinds then it gives rise to an aerodynamic yaw angle (ψ). This parameter will also affect how drag coefficient is defined. Ref [17] claims that plotting Cd with respect to the square of the yaw angle (between 0-15 degrees), yields in a linear relationship. In addition, the y-intercept is Cd0 and the slope is a constant K. [17], [18], [19] used equation (2.2) to represent the aerodynamic drag as a function of velocity with the effect of crosswinds.

$$C_D = C_{D_0} + K\psi^2 \qquad (2.1)$$

$$F_{aero}(v) = \frac{1}{2}\rho A\left(C_{D_0} + K\psi^2\right) * V_r^2 \qquad (2.2)$$

Y is yaw angle

Vr is airspeed

Over time people have make an effort to improve these aerodynamic models. For example, Altinisik [20] derived a different second order equation for estimating the aerodynamic drag coefficient as a function of yaw angle. He tested his equation by doing a coast-down test and calibrating the wind tunnel and CFD calculations for three vehicle designs. The coast-down predicted the drag coefficient 5-8% less than the wind tunnel. Altinisik suggested this was due to the rotating wheel effect.

In general, however, SAE J2263 states that the drag coefficient is represented by equation (2.3). This equation is based on studies conducted by Buckley which had sufficient repeatability to enable a good correlation between track and wind tunnel data [21].

$$C_d = a_0 + a_1\psi + a_2\psi^2 + a_3\psi^3 + a_4\psi^4 \quad (2.3)$$

$$F_{aero} = \frac{1}{2}\rho A V_r^2 (a_0 + a_1\psi + a_2\psi^2 + a_3\psi^3 + a_4\psi^4) \quad (2.4)$$

The SAE J2263 complete road load equation is the following:

$$F_{load} = A_m + B_m V + C_m V^2 + \frac{1}{2}\rho A V_r^2 (a_0 + a_1\psi + a_2\psi^2 + a_3\psi^3 + a_4\psi^4) \pm Mg\frac{dh}{ds} \quad (2.5)$$

A laboratory or wind tunnel has certain limitations in representing an accurate environment of real conditions. These limitations will generate a discrepancy between track and lab results. Passmore [17] evaluated aerodynamic drag in a test track and wind tunnel with different vehicle configurations to try to quantify its effects. He obtained results with a notable difference between track and laboratory data, showing that the wind tunnel under-predicts drag. Similar studies have shown comparable results with respect to the different outputs between wind tunnel and track [18].

There are three main constraints in a wind tunnel that are difficult to account for. Even though these conditions have a relatively small error percentage, it is important to understand and try to improve them.

First, in traditional wind tunnels the wheels of the test vehicle do not rotate causing an error in the drag of the wheels. Multiple studies have shown that the total vehicle drag reduces

with rotation of the wheels [22] [23]. The majority of the current wind tunnels incorporate wheel rotation during their tests, but there is still ongoing research trying to quantify its effect.

Second, stationary versus moving belts in wind tunnels generate different outputs. When the ground is fixed relative to the vehicle it allows an unrepresentative boundary layer to develop [24]. Howell [24] compared coast-down test data with fix and moving ground wind tunnels. The average drag coefficient in the stationary and moving wind tunnel was 0.009 and 0.002 less than the coast-down data, respectively. A wind tunnel with moving belt represents more accurate real driving conditions, the only drawback is that it is quite expensive to build.

A third constraint is the fact that a wind tunnel is in a closed environment. Due to this, there needs to be a blockage correction factor to represent more realistic airflow conditions as in a real road. Sahini [25] derived a model to predict wind tunnel blockages effects on pressure and velocity distributions. The blockage correction equations demonstrated a good correlation for drag coefficient and test section height.

Iwase, Yamada and Koga [26] derived a correction coefficient (b) for aerodynamic drag for wind tunnel testing in equation (2.6). [26] validated its derived equation by comparing road loads with coast-down tests for 8 vehicles.

$$b = e * x \qquad (2.6)$$

$$e = (1 - BR)^2 \qquad (2.7)$$

$x =$ the effect of other factors except blockage effect, such as tire rotation and the existence of boundary layer on the wind tunnel floor

$BR =$blockage ratio = vehicle frontal area/test section area

Besides being difficult to simulate exact real drive conditions in a laboratory, it has also been observed that there are inconsistencies between different wind tunnels. Le Good [17] states that there is a degree of scatter in the data from various wind tunnels. Correlation tests done during the 1980s showed an approximate 5% variation in drag coefficient values between wind tunnels [24].

For instance, Walter [27] cites the example of a vehicle test with the addition of a rear spoiler. In one tunnel this resulted in a 5% drag reduction—probably enough to justify adding the spoiler—whereas another tunnel indicated only a 1% drag reduction [27]. Similarly, Passmore and Le Good [18] indicated that the variation in drag coefficient between different wind tunnels could exceed 0.020. From the mentioned studies, it can be concluded that the differences between wind tunnel and track data are both configuration and tunnel dependent.

2.2 Parasitic Forces

Parasitic or drivetrain components are the rotating components of a vehicle mechanically connected to the driving wheels when the transmission is in neutral gear. Some of these components are the brake disks/drums, driveshaft, transmission, differential, output shaft,

propeller shaft, etc. These losses have a smaller percentage than aerodynamic or rolling resistance in the overall forces, but they are still high enough that it is important to quantify them.

Every vehicle experiences different levels of parasitic losses since it is determined by its design of transmission and driveline components. Commonly, industry tries to measure this value from a dynamometer test or with wheel torque meters but then they need to subtract rolling resistance from this value. This could generate an error if rolling resistance is not properly calculated.

The previously mentioned SAE paper defines the mechanical drag (in the road load equation) as the combination of rolling resistance and friction in the driveline and non-drive axle components. It is represented by a three-term polynomial with respect to speed:

$$F_{mech} = A_m + B_m V + C_m V^2 \qquad (2.8)$$

However, multiple papers have studied the importance and methodology for measuring the driveline losses separated from rolling resistance. Most of the papers that focus on measuring parasitic losses, do it by doing a "coast-down in the air". In general, a vehicle is jacked up off the floor to ensure isolation of the wheels from rolling resistance effects, and the drivetrain is warmed up until equilibrium conditions. Then, the tires are brought up to a desired speed and the drivetrain is decoupled from the transmission. The current studies

that adopt this methodology do not explain if there is any counter-effect due to gravity and having the vehicle in the air.

Singh, Jadhav, Vishe and Gopalakrishna [28] followed the above methodology for measuring the frictional losses for a vehicle in coasting mode. Based on experimental data, [28] established that a linear model was sufficient for describing frictional losses. The comparison in losses between two different vehicles is shown in figure (2.2). There is a noticeable difference in driveline losses.

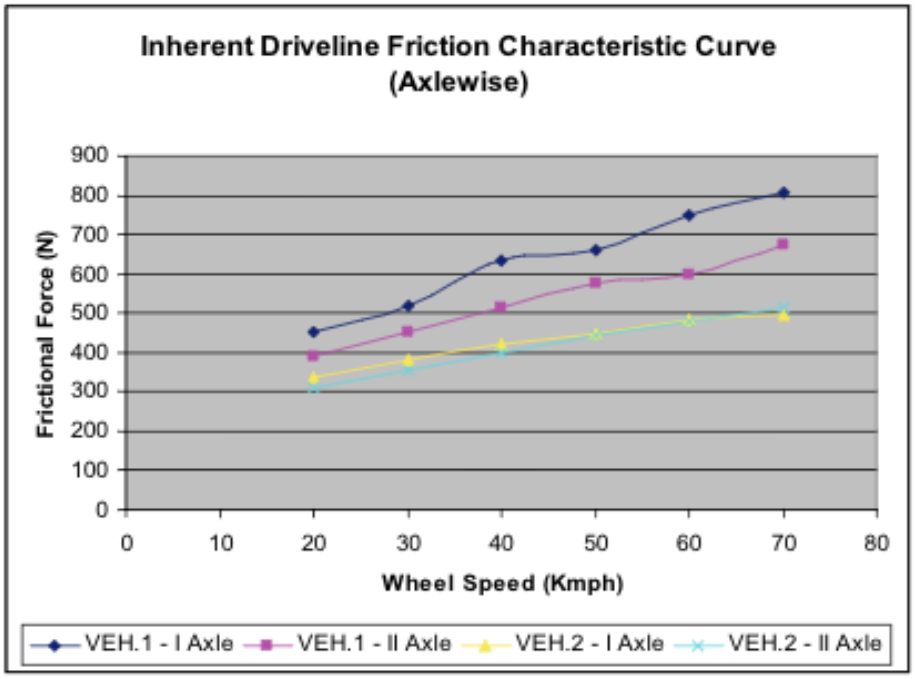

Figure 2-2 Driveline losses [28]

On the other hand, Dayman [29] did a similar test with one vehicle and obtained a non-linear relation between the drivetrain losses and vehicle speed. Nevertheless, Dayman only

had three data points during his study which leads to certain uncertainties of his results in comparison to Singh's study.

Other studies have quantified parasitic losses in two separate parts –transmission and un-driven-wheel losses [18], [30]. After collecting experimental data, Passmore and Good [31] modeled the transmission losses as a quadratic function and the un-driven wheel losses as a linear relation with respect to speed. In addition, [31] demonstrated that the driveline losses not only depend on vehicle speed, but also on oil temperature.

2.3 Rolling Resistance

The second parameter that contributes the most to the total road load is rolling resistance. Rolling resistance in tires is primarily caused by the hysteresis in tire materials due to the cyclical deformation of the tire while rolling. The higher the hysteresis losses, the higher the rolling resistance force. In general, rolling resistance is defined as the energy consumed by a tire per unit of distance covered [32].

Generally, rolling resistance coefficient (RRC) is defined as the ratio of rolling resistance to the normal load. However, RRC is affected by several different parameters, this ranges from the properties of the tire (size, material) to its operating condition (inflation pressure, temperature, speed, surface of the road, normal load, etc).

Similar to the aerodynamic drag force, there are different ways of measuring rolling resistance. As mentioned before, a coast-down test takes all the road load forces including

rolling resistance into account. Then for isolating or replicating rolling resistance, it can be done in a laboratory with a chassis dynamometer or drum test. For laboratory testing, a correction coefficient for the curvature effect compared to a flat road is applied.

An important requirement for doing any coast-down or laboratory test is to make sure that the tires have reached equilibrium conditions. A true equilibrium requires that temperature and pressure be stabilized inside the tire. Fuller, Hal and Conant [33] studied how much time it takes a tire to reach equilibrium conditions. [33] tested the running time of various types of tires at 80% of the maximum load and at a speed of 80 km/h. Table (2.1) shows the results of different tests and it was concluded that an average warm-up of 20-25 minutes was sufficient to reach equilibrium for passenger cars.

Table 2-1 Time for tires to warm up

Tires	Number of tests	Range [min]	Average [min]
P195/75 R14	60	16-26	20.7
E78-14	30	14-28	20.6
ER 78-14	10	16-26	20.2
P195/75O14	9	22-30	25.5

Longer times would be necessary for larger tires. According to Michelin, the process of reaching equilibrium condition could take up to two hours for truck tires [32]. SAE J2263

stablished a required 30-minute operation at 80 km/h to precondition passenger vehicle and tires for a coast-down [14].

2.3.1 Speed and Load

Rolling resistance coefficient is relatively constant with respect to speeds up to 100-120 km/h. After that point, RRC slightly increases with speed. The sudden increase in RRC is due to increase in aerodynamic drag of the rotating tire and strong vibrations at high speeds [32].The mathematical models representing RRC as a function of speed varies widely, but in most cases a linear or quadratic function is used [34] [35] [29].

On hard surfaces (i.e. concrete), RRC decreases rapidly as tire pressure increases. This occurs because inflation pressure affects the flexibility of the tire. With higher inflation pressure, the deformation of the tire with respect to the ground decreases generating lower hysteresis losses [32].

Under other surfaces, RRC acts differently. Figure (2.3) represents how RRC changes with respect to different surfaces. Under deformable surfaces (sand), RRC is considerably higher than under hard surfaces. RRC is not only affected by the road surface material but also by the diameter of the tire. Figure (8) also demonstrates that as tire diameter increases, the coefficient of rolling resistance decreases. In [Michelin, 2003] it is stated that 10 mm of increase in rim diameter reduces RRC by 1 %,

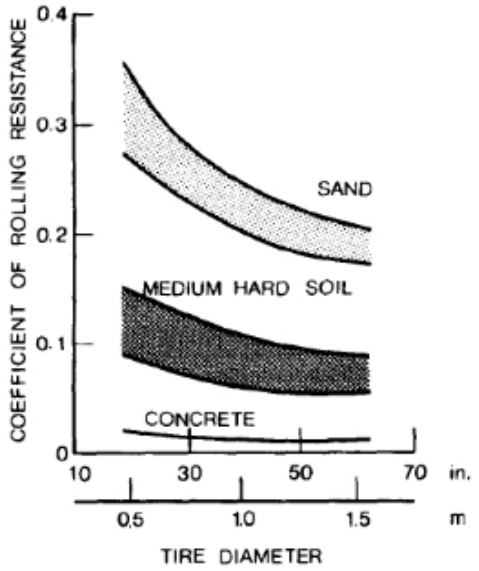

Figure 2-3 RRC versus tire diameter [67]

Based on some of the mentioned relationships, Grover [36] developed a function for rolling resistance based on pressure, load and speed. His model is currently used in the SAE J2452 recommended practice for measuring tire rolling resistance in a laboratory. The complete SAE equation for rolling resistance in a laboratory is the following:

$$RR = P^{\alpha} L^{\beta} (A + BV + CV^2) \qquad (2.9)$$

P inflation pressure (kPa)

L applied vertical load (N)

V speed (kph)

a,b,c coefficients

α, β exponents

However, the previous model does not take into account other factors impacting rolling resistance. For example, previous research has shown the impact of doing tests in different ambient air temperatures [37]. In 2003, Michelin [32] identified that the variation of rolling resistance as a function of ambient temperature was not linear. However, between the range of 10 and 40°C, a change of 1°C corresponds to a change in rolling resistance of 0.6%. Based on these studies, the ISO 28580 suggested a temperature correction to a reference temperature of 25°C with equation (2.10).

$$F_{r25} = RR[1 + K(t_{amb} - 25)] \qquad (2.10)$$

RR is rolling resistance [N]

K is equal to 0.008 for passenger tire

K is equal to 0.01 for truck and bus tires with a load index of 121 or lower

K is equal to 0.006 for truck and bus tires with load index 122 or above

t_{amb} is the ambient temperature, in degrees Celsius

2.3.2 Road surface

Another factor that has been traditionally neglected, at least in standards, is the lack of pavement perspective. Current standards do not take into account the effect of road texture degradation with respect to RRC. There is not a standard of how often companies should repave the roads in which they do testing; automakers repave their roads every 2-5 years, a range that could affect results.

Pavement texture is defined as the deviation of a pavement texture from a true surface within a specified wavelength range [38]. Surface texture can affect road characteristics and vehicle performance in multiple areas such as: noise in vehicles, tire friction, tire wear, rolling resistance, etc. Figure (2.4) represents the wavelengths and spatial frequency of each texture, and the impact that each one has on different parameters according to [39].

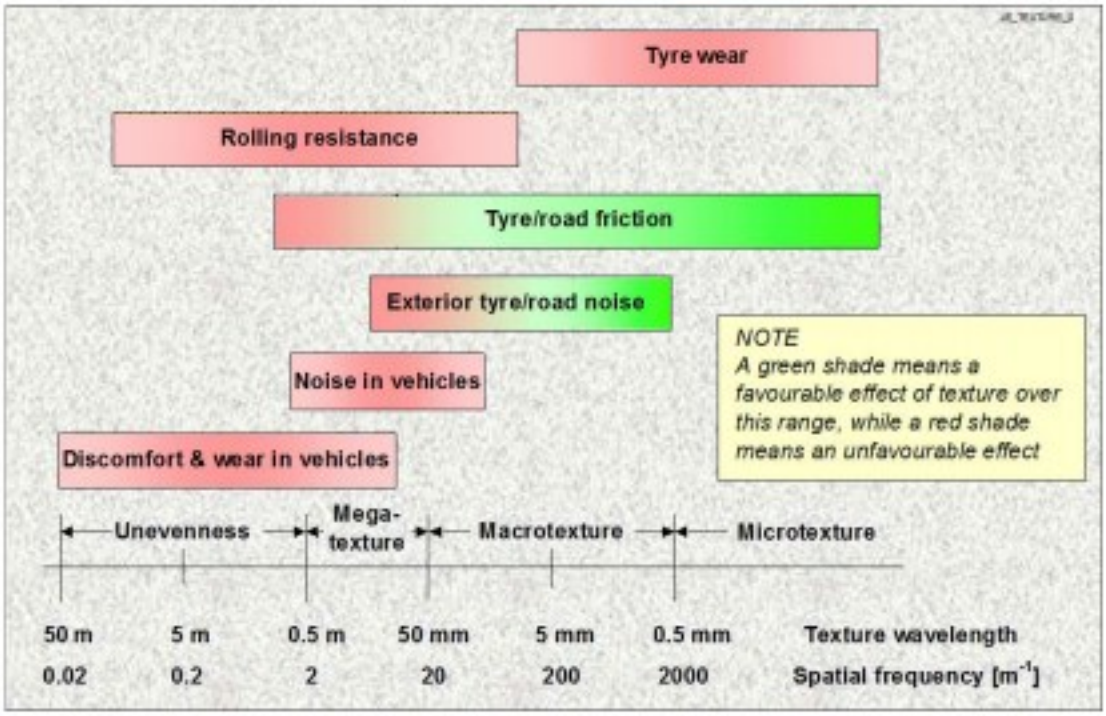

Figure 2-4 Surface texture wavelengths [40]

When a specific road is paved, its texture will not affect as much rolling resistance since the road is as smooth as possible. However, with time the weight of the vehicles and weather effects will cause a deformation on the road. As the road degrades, this is reflected in an increase in the measurement of each wavelength.

Surface texture measurements have been standardized and are globally used. Currently, the most common measurement for macrotexture is Mean Profile Depth (MPD). This measurement can be calculated with stationary or moving laser sensors, which records the profile curve in a two or three-dimensional representation. The current standard, ISO 13473-1, states that MPD should be calculated from a sample baseline length of 100mm, which is divided in two equal halves. Then, the peak value of each half is identified and

the average between the two peaks is the MPD of that specific sample. If the complete road profile is longer than 100mm, this calculation should be repeated for each 100mm baseline and the average of all the samples will determine the MPD of the profile [38]. Figure (2.5) represents the MPD computation.

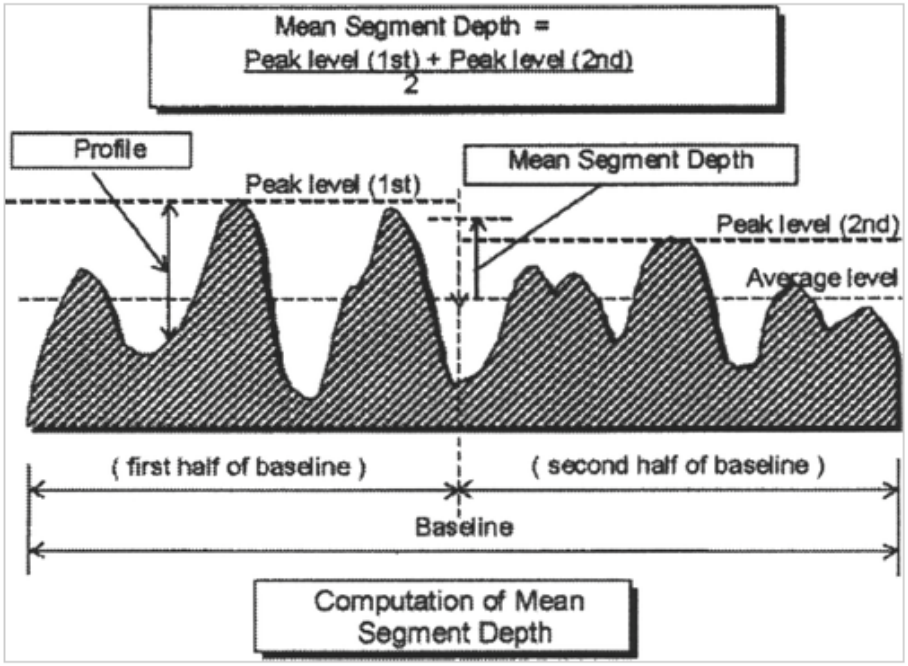

Figure 2-5 MPD representation [41]

Instead, for measuring texture unevenness, the World bank developed the international roughness index (IRI) during the 1980s. IRI is the most common road roughness index used to equally evaluate infrastructure. The commonly recommended units are meters per kilometer (m/km) or millimeters per meter (mm/m) [42]. IRI measurement is calculated by using a quarter-car vehicle mathematical model [43], and it is specified in the international

standard ASTM E1926-08. Figure (2.6) represents IRI roughness scale according to Sayers [44].

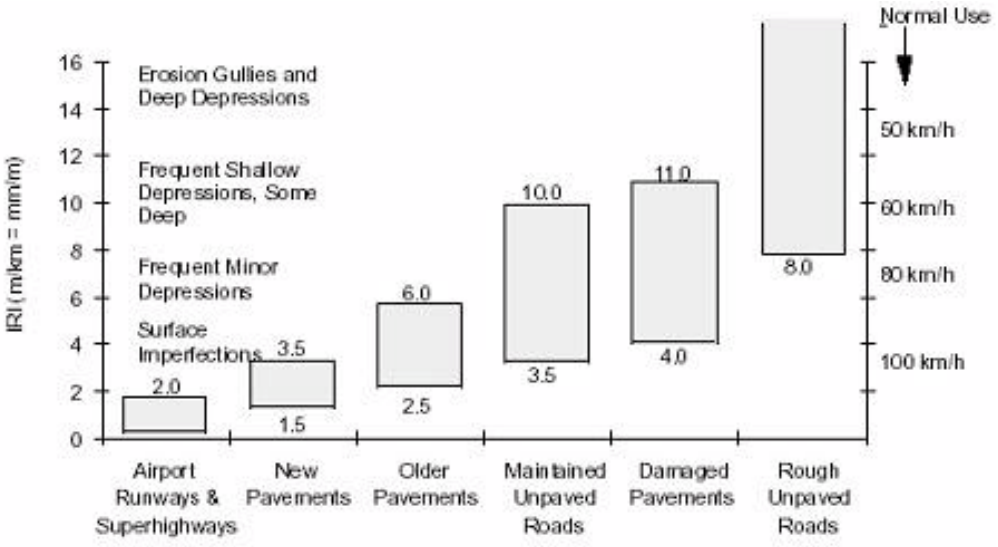

Figure 2-6 IRI in different roads [44]

Since road surface affects rolling resistance, it will also affect directly fuel consumption. As the road surface degrades, RRC increases, making the road load increase and causing fuel consumption to also increases. Laganier and Lucas [45] measured rolling resistance in different roads and calculated the equivalent fuel consumption. [45] developed a relation of extra fuel consumption due to different levels of unevenness. Figure (2.7) shows the final results with respect to a car that had an average fuel consumption of 7 liters/100 km. Laganier and Lucas demonstrated that there is an increase in up to 6% for the specific vehicle when the road was at its "worst" condition.

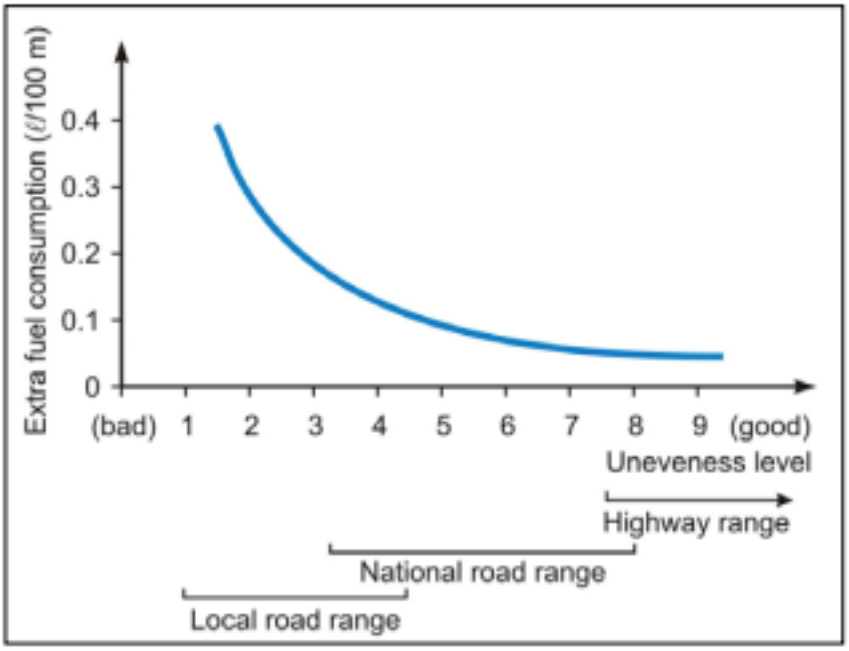

Figure 2-7 Extra fuel consumption according to road unevenness level [45]

For the macrotexture level, there have also been multiple studies of how it affects RRC [34]. For instance, Sandberg [46] tested approximately 100 car tires in a drum facility in Poland. Two very different drum surfaces were used, one was a smooth sandpaper and the other a surface dressing with 11 mm chippings. The idea of the study was to see if there was a relation between MPD and speed, and between MPD and RRC. Figure (2.8) shows that RRC doesn't change much by varying the tire rolling speed. [46] reported that the sandpaper surface and surface dressing had estimated macrotexture MPDs of 0.12 and 2.4mm, respectively. The distinction in MPD values is translated into a clear difference in RRC between the two surfaces.

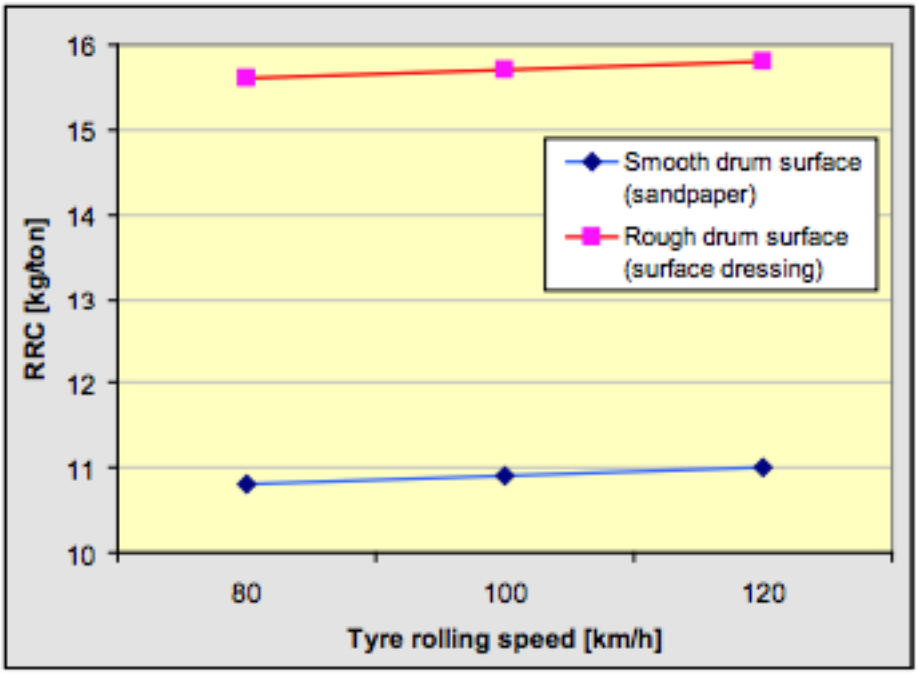

Figure 2-8 RRC based on speed and surface texture [46]

On the other hand, there is a limited amount of studies and papers that cover the effects of microtexture. As observed in figure (2.4), microtexture is believed by some to not affect rolling resistance. However, since microtexture is still causing a certain deflection on the tire, it should also be affecting rolling resistance (in a smaller percentage than the other wavelengths) [47].

Finally, a project conducted at Swedish National Road and Transport Research Institute (VTI) performed various coast-down tests in both light and heavy vehicles [48]. These tests made possible to determine the relative contributions of energy losses due to road surface. Figure (2.9) demonstrates the influence that road surface (MPD and IRI component) have on a vehicle. [48] did not specify the initial condition of the road.

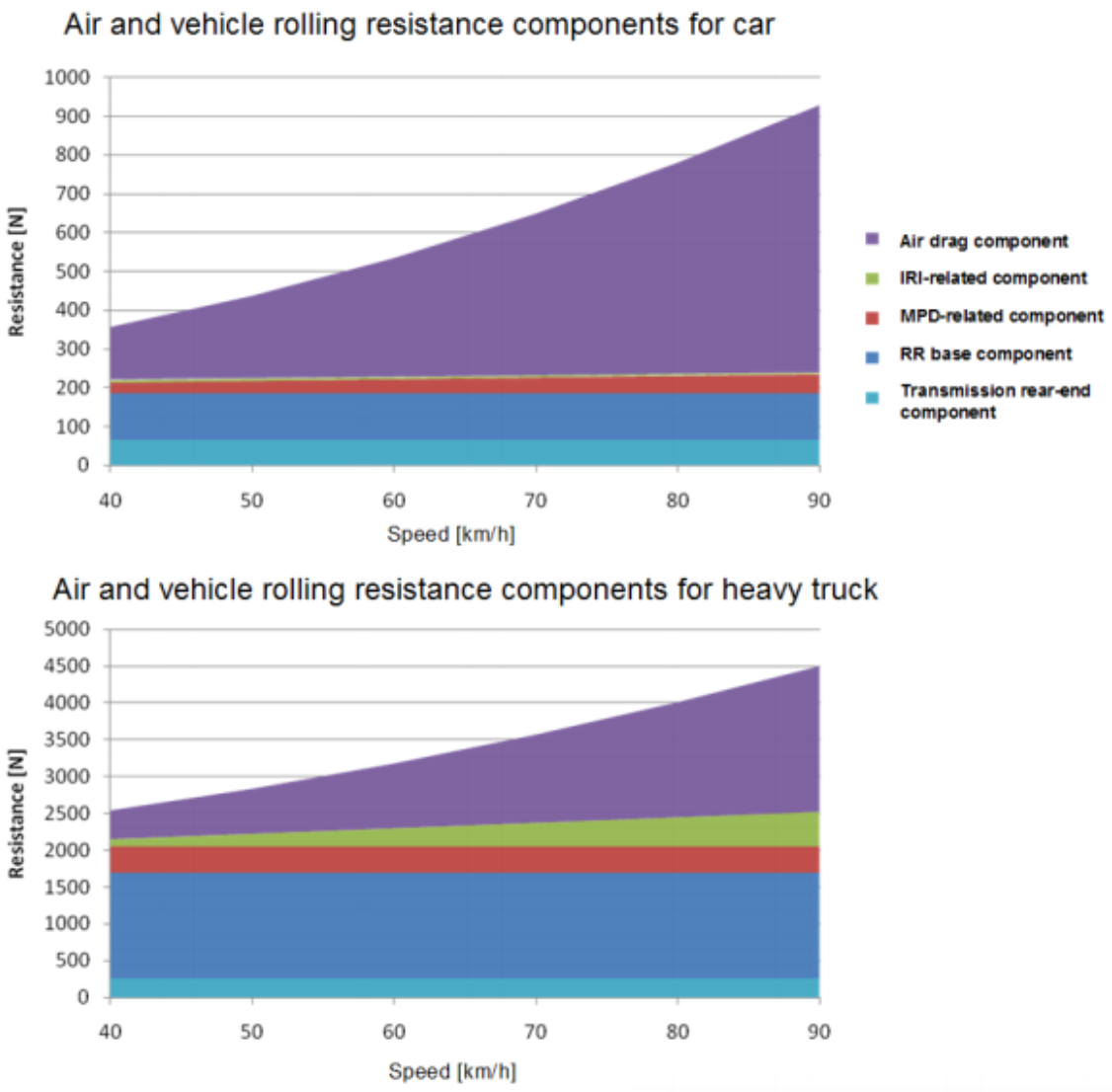

Figure 2-9 Road load with MPD impact [48]

As it has been studied, there are three main components affecting the road load in a vehicle. Aerodynamic drag depends on wind speed, speed direction and ambient conditions. Driveline losses vary according to the transmission and components design, and lubricant properties. Lastly, according to the standards of rolling resistance, it depends on pressure, load and speed. However, there is evidence that an important element has not been

incorporated, which is the condition of the road surface. This parameter could generate significant changes in the RRC, and as a result in the fuel consumption.

This thesis studies the impact of road degradation as a function of micro- and macrotexture. The main objective is to quantify how much each of the mentioned wavelengths change during a specific span of time in a transited road. In the next chapter, the methodology for measuring each wavelength and its process is explained in detail.

Chapter 3 : Methodology

An experimental study was conducted as part of this thesis in a proving ground near Phoenix, Arizona. The main objective of this study was to collect data regarding the road surface of a 1.5-year old road before and after it was repaved. The data was obtained with a static optical profilometer called Laser Texture Scanner (LTS). The LTS is capable of measuring micro- and macrotexture wavelengths. In addition, the raw data can be converted into the standard texture metric called mean profile depth (MPD). MPD can be used for quantifying how much the rolling resistance properties changed with respect to two different wavelengths. This chapter goes over the methodology of how micro- and macrotexture were measured for a further analysis.

3.1 A review of surface roughness measurements

The methods and standards for characterizing road surface texture have changed throughout the years. The most traditional method is the Sand Patch Test, which follows the ASTM E 965 standard [49]. For this method, a known volume of glass beads is spread evenly over the test surface forming a circle. After filling all the surface voids, the diameter

of the circle is measured in different axes and averaged. Then, this value is used to calculate the mean texture depth (MTD). Other traditional methods are the outflow meter and the grease patch [50].

However, the previously mentioned methods provide an indirect measurement of the surface depth at a discrete spot and are not sensitive to the microtexture level [50]. In order to measure more efficiently and at higher resolutions, dynamic and static lasers have been developed for measuring various surface wavelengths. Currently, profilometry is one of the main techniques for extracting topographical data from a surface. This method is highly adopted due to its high resolution and easy implementation. Profilometers can detect road surface texture in wavelengths as small as 1 micron (1,000,000 cycles/meter) [51].

Profilometers are divided mainly in two categories: contact and non-contact devices. Contact or stylus profilometers physically move a probe along a surface to quantify the surface height. This is performed with a feedback loop that monitors the force from the sample pushing up against the probe while it is scanning the surface. Even though this type of profilometer gives high resolution, it is very sensitive to soft surfaces and the probe could potentially get contaminated by the surface.

Non-contact or optical profilometers use light instead of a physical probe. Optical profiling uses the wave properties of light to compare the optical path difference between a test surface and a reference surface [52]. In general, inside the optical profilometer a light beam is split, one part reflects towards the test surface and the other half is reflected to a reference mirror. The phase difference between the reflected beams of the test surface and the reference mirror is dependent on the distance between the test surface and reference mirror.

Based on this difference it is possible to quantify the profile of a surface and reproduce 3D images. Figure (3.1) represents how the optical profilometer works.

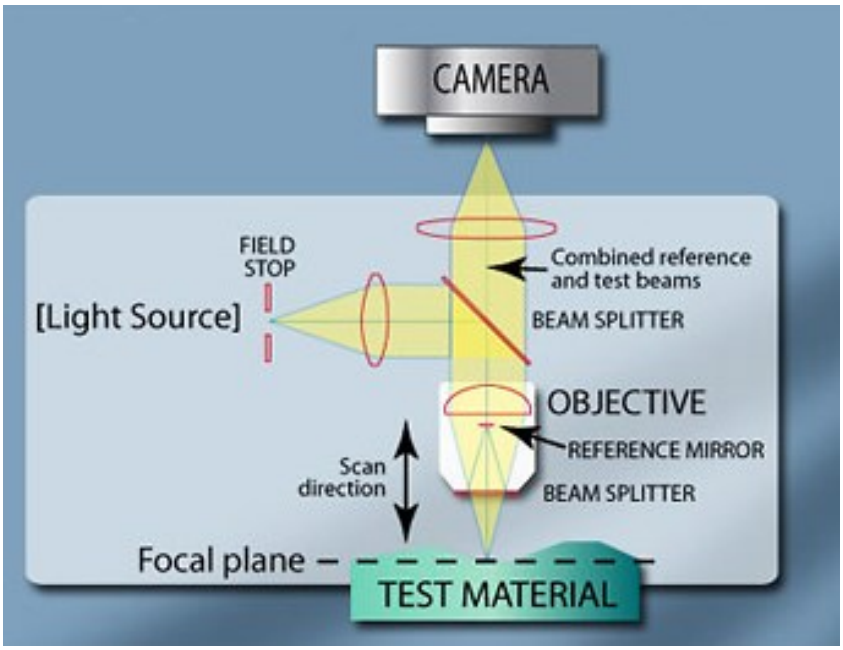

Figure 3-1 Optical profilometer [52]

3.2 Laser Texture Scanner and error analysis

Measurements of the road surface texture were taken with a Laser Texture Scanner (LTS) made by Ames Engineering, as shown in figure (3.2). The LTS 9200 is an optical profilometer designed to measure road surface in a 3-dimensional area scan. This machine uses a moving linear rail system to accurately move a laser over a specific surface.

The LTS is designed to measure the two decades (50mm to 0.5mm) in the macrotexture waveband and one decade (0.5mm to 0.05mm) of the microtexture waveband [53]. Texture in these wavebands is useful in determining surface friction and tire noise measurements [53]. In addition, the scanner is a stand-alone unit that can be placed on the surface on three-point contact, and it scans the surface in multiple lines to measure index calculations. Different index calculations are available for the LTS to compute, such as: mean profile depth (MPD), estimated texture depth, texture profile index, etc. Based on multiple studies, the most common and useful parameter to quantify and compare surface texture is MPD [51] [54]. As a result, this study mainly focuses on the characterization of MPD in the track.

One scan of the LTS has an area of 3x4 inches, which is divided in a specific number of lines depending on the precision and accuracy that the user wants. The range of lines is between 10 to 1200 per scan area. However, the more lines used the longer it will take for scanning. At a maximum resolution, one scan area will take approximately 2 hours and it will have ~ 4.3 million data points.

Figure 3-2 Laser Texture Scanner

Even though the LTS records millions of data points, the understanding of the LTS's accuracy is essential since the calculation of MPD is sensitive to outliers. The uncertainty error is expected to affect more the microtexture wavelength, because this wavelength is 10 times smaller in magnitude than the macrotexture. Table (2) displays some of the system specifications of the LTS.

Table 3-1 LTS specifications [53]

Laser Dot Size	0.05 mm (0.00197 inch)
Vertical Sample Resolution	0.01 mm (0.0004 inch)
Horizontal Sample Spacing	0.015 mm (0.0006 inch)
Profile Wavelength Range	0.03-50 mm (0.0012- 1.97 inch)

Based on table (3.1) the vertical resolution (surface height) can be detected every 0.0004 inch with the LTS 9200. The MPD in the macrotexture data obtained from the LTS is in the range between 0.0089-0.0191 inches (including the data from before and after repaved). Therefore, there is a tolerance error of $MPD_{macro} \pm 0.0004\ inches$, which in the worst-case scenario corresponds to a 4.5% error.

On the other hand, microtexture is a smaller wavelength and is more affected by the limited resolution. The MPD microtexture data obtained is in the range between $1.9 * 10^{-3} - 4.1 * 10^{-3}\ inches$. The tolerance error would be $MPD_{micro} \pm 0.0004\ inches$, which in the worst-case scenario corresponds to a 21% error. There are newer versions of Ames Engineering LTS with higher resolution and accuracy, unfortunately they were not available during this project.

Table (3.1) also shows the available profile wavelength range, which covers both micro- and macrotexture. To be able to analyze both wavelengths, the entire range was selected to obtain the raw data. Afterwards, different filters were applied to smooth and separate the data between wavelengths. More details are discussed in the next section.

3.3 Measurements of road texture at a proving ground

Since one of the main objectives of this project is to analyze the degradation of a road surface over a certain period of time, arrangements were made to conduct a set of several experiments at a proving ground. The aim of these experiments was to collect samples of

the surface texture in a specific road before and after it was repaved to understand how this could affect a coast-down test. Figure (3.3) depicts the proving grounds where the tests were done; specifically, measurements were taken in the straightaway in the bottom of the figure.

The straightaway is use daily for doing coast-down tests of multiple vehicles. Due to this, the road surface must meet the require characteristics for doing coast-downs. Effects of an incline surface can be neglected since the road has a grade of 0 degrees. Also, since this road is primarily used for coast-downs, it is transited by passenger cars and light trucks, but not by heavy vehicles. Considering that the proving grounds are located near Phoenix, Arizona, the impact of snow on the road does not have to be considered.

The straightaway has one lane of 1.8 miles in length (short leg) going from south to north, and another lane of 2.0 miles in length (long leg) going from north to south. Both lanes are connected by two curvature sections, one at the end of each leg. Throughout each leg there are mile posts every 0.1 miles for reference purposes. Figure (3.4) shows each leg and one of the curvature sections for better visualization.

Figure 3-3 Proving Grounds overview

Figure 3-4 Proving grounds zoom-in

In addition, each leg is divided in 3 sections -left, right and center lane. At this proving ground, vehicles drive only in the center lane due to requirements of not changing of lane

during a coast-down test. Vehicles only go to the right or left lane if they need to stop or in case of an emergency. Furthermore, the center lane is the only part of the straightaway that is approximately repaved every 2 years because it is the only part where coast-down tests happen.

It is important to understand that the curvature section and the right/left lane have not been repaved in almost 4 years when the measurements were taken for this project. Figure (3.5) shows a part of the long leg in which the darkest lane corresponds to the center lane, since its newer than the other two lanes.

Figure 3-5 Long leg at Proving Grounds

During November of 2016, the center lane of both the long and short leg was repaved. Then, in April of 2018 the center lane was repaved again. The proving grounds were visited in two occasions; the first time was a couple of days before it was repaved in April 2018, and the second time in June of 2018. Throughout each visit, multiple measurements were collected of each leg and one measurement was taken from the curvature section for comparing results with a 4-year-old road.

Before going to Arizona, a small study was performed in order to identify the minimum number of lines per scan area necessary to have reliable results. This was done because there was a limited amount of time allowed at the proving grounds. Table (3.2) represents the time for scanning an arbitrary surface with different lines and the MPD value for each case.

Table 3-2 LTS scan duration

No. Lines	**10**	**100**	**200**	**300**	**400**	**600**	**1200**
Time	90 s	10 min	20 min	30 min	40 min	60 min	120 min
MPD	0.0238	0.0264	0.0263	0.0263	0.2649	0.0268	0.0266

Based on table (3.2), the error percentage of MPD between 100 and 1200 lines is less than 1%. This difference is small enough to get approximate accurate results with 100 lines. This result is also supported by [55], which performed a similar test with a different version

of a LTS. To be able to collect as many measurements as possible, it was decided to use 100 lines as the laser scanner specification. The laser texture scanner used the selected number of lines and equally spaced them over the width.

Also, the LTS has the ability to control how much power laser it uses. Half power setting is better when scanning bright white surfaces with no sunlight striking the test surface area. Direct sunlight will cause spike errors to occur and will distort the data. Alternatively, full power setting works better for very dark surfaces or when scanning outside under the sunlight. For this project, full power laser setting was selected due to the surface that was scanned.

Figure (3.6) represents how each measurement at each specific mile post was taken in the center lane. Each red square represents one measurement taken by the LTS. The right and left red square aim to match with the right and left wheel of the vehicle, respectively. The center red square is located in the middle of the lane, where the vehicle is not supposed to drive over. The center square is meant to study the weather effect compared to the right/left measurements. Based on this setup, in the first mile post, the distance of each scan with respect to the side of the lane was recorded and used for consistency in the following scans. In addition, before each scan was taken, the surface was swept to make sure there was not something obstructing or influencing the results.

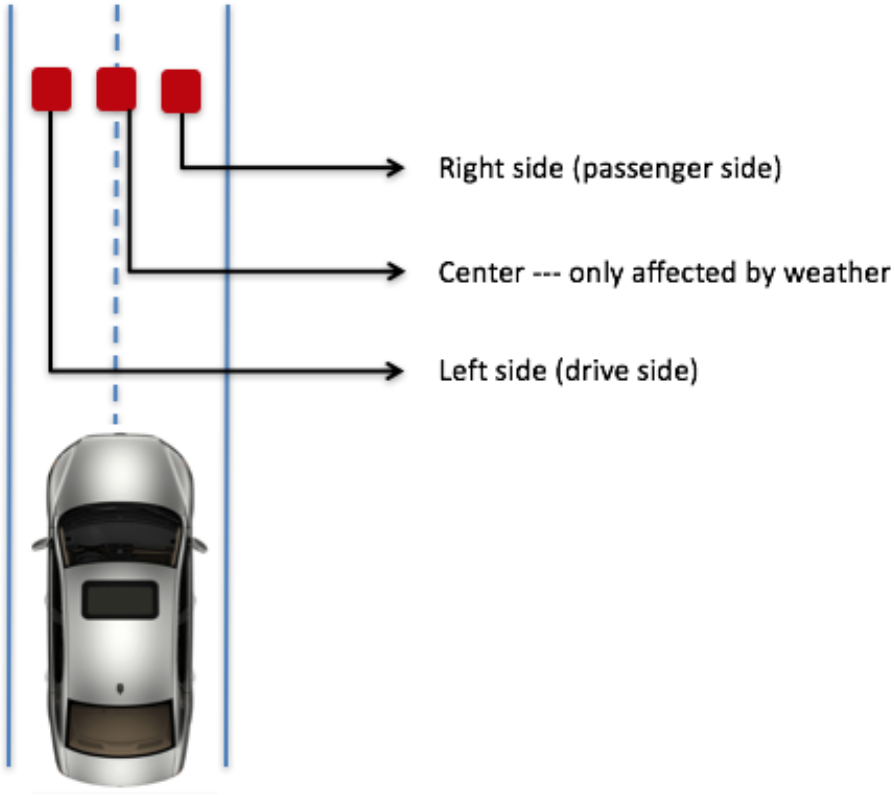

Figure 3-6 Location of LTS scans

Table (3.3) displays in which specific mile posts the measurements were taken for both the long and short leg. The same measurements were aimed to be taken during both visits for consistency. Unfortunately, during the measurements of the long leg after the road was repaved, a sandstorm took place and few points were missing. Also, there is one extra data point taken in one of the curvatures to see the surface texture of a 4-year-old road. The curvature data point was taken in a spot where vehicles would not normally drive though, the main purpose of this data point is to analyze the effect of road degradation due to weather.

Table 3-3 Mile post measurements

Short Leg	
Mile Post	**Wheel Paths**
0.0	L, R
0.2	L,R
0.4	L, R
0.6	L,R
0.8	L, R
1.0	L,R
1.2	L, R, C
1.23	C
1.26	C
1.4	L,R
1.6	L, R
1.7	L, R

Long Leg	
Mile Post	**Wheel Paths***
0.0	L, R
0.2	L, R
0.4	L, R
0.6	L, R
0.8	L, R
1.0	L, R
1.2	L,R
1.3	C
1.33	C
1.36	C
1.4	L,R
1.6	L,R
1.8	L,R
2.0	L,R

*L = left wheel path
R= right wheel path
C= center of the lane

In addition, surface texture data from a contractor was available for comparing and validating the LTS's data. The contractor's data was collected by using a different device called RoboTex as shown in figure (3.7). RoboTex is a mobile robotic-based texture measuring device that utilizes a line laser and produces 3D images. This device is capable of measuring a continuous pavement strip, instead of a single area like the LTS. RoboTex is designed to measure any type of pavements including those with surface treatments. However, this device can only measure wavelengths greater than 0.5mm (i.e. macrotexture and above). The RoboTex took measurements in the same mile posts that the LTS did to be able to compare.

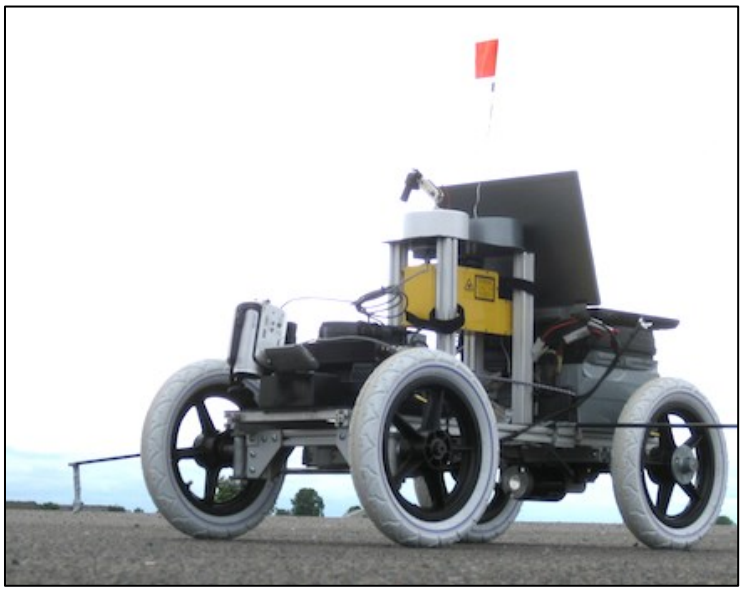

Figure 3-7 RoboTex [56]

3.4 Summary

This chapter provides an overview of different possible methods to characterize a surface texture. The optical profilometer LTS outstands other methods due to its high resolution and easy implementation for this project. After visiting twice the proving grounds in Arizona, 86 measurements were obtained in total with the LTS. There is a small difference in the number of measurements between before and after the road was repaved due to a sandstorm. The LTS allows the user to download the raw data or use the scanner's built-in software. The following chapter covers how the MATLAB^{TM} code was structured for post-processing the raw data and analyzing it.

Chapter 4 : Data Analysis

This chapter introduces spike errors as a possible source of error inherent to optical profilometers, and how to minimize their impact on the data. Then, raw and processed data is displayed to have a first sight of the complete set of data. As previously mentioned, a MATLAB^{TM} code was developed in order to process the data by following the MPD's calculation standards [57]. Both the LTS and RoboTex data are processed with the MATLAB^{TM} code for validation and comparison purposes. In addition, different analysis are performed on the data to be able to develop a mathematical equation to represent road surface degradation per day for each wavelength.

4.1 Spike Errors

The functioning behavior of a profilometer or laser could deviate from the ideal conditions due to external factors. One of the most commons issues encountered when using optical systems, like a profilometer, is the appearance of "spike errors". These spikes usually arise from two ways and could impact the results. First, it could be due to extreme gradients in the surface (sharp edges), which cause the reflecting laser to go in the wrong angle. Second, a spike error can appear as a result of optical aberrations.

Aberration is a property of optical systems that makes the light to be spread out rather than focused to a single point; it could cause an image to be blurred or distorted. Figure (4.1) represents raw data with some spike errors.

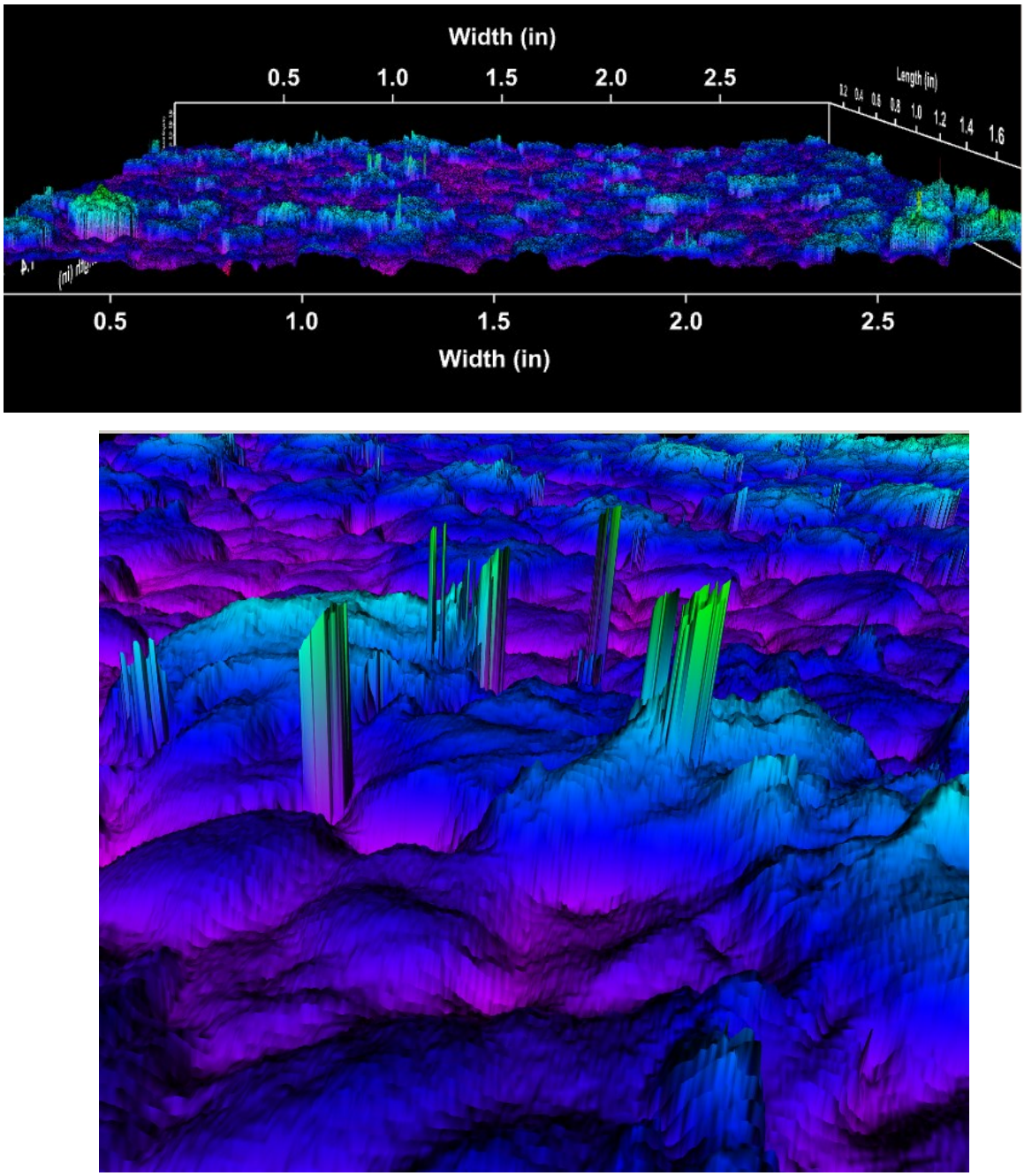

Figure 4-1 Spike Errors

Spike errors have been quantified to approximately be between 1.1x – 10x the original signal (absolute value) [51]. The larger the spike error the easier it is to detect and eliminate. Even though small magnitude spike errors do not have a high impact on surface parameter calculations, it is still preferable to remove them from the data set.

Usually spike errors are considered to be outliers of the data, and multiple approaches have been proposed for removing them. Application of morphological filters or detection of points of high slopes are some examples [58]. In other studies, the distribution of texture measurements fits a gaussian distribution, and this has allowed to easily detect outliers by examining the tails of the distribution [59]. However, Walton [51] showed evidence that texture height distributions do not follow a specific distribution when measuring at sufficiently high resolutions. Figure (4.2) shows an arbitrary set of data from the LTS and how it does not follow a normal distribution. Consequently, a different approach needs to be taken to identify outliers.

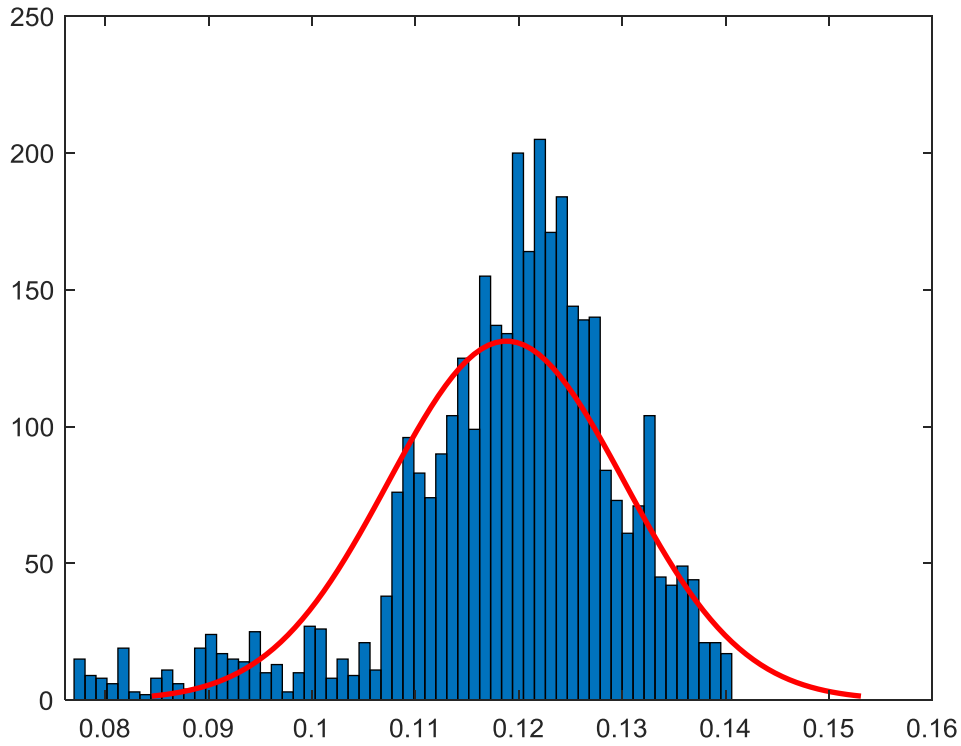

Figure 4-2 Raw data histogram

4.2 Data processing:

As previously noted, there is not a comprehensive methodology or algorithm for detecting spike errors in optical profilometries. Therefore, based on literature review and MPD standards, the following procedure was applied to process the raw data and reduced the spike errors.

- The mean value of the surface was subtracted from each data point to adjust the reference plane to zero.

- A Butterworth's filter of 3rd order was applied to separate the micro- and macrotexture data. For the macrotexture, a low pass filter was applied with a cut-off of 2000 cycles per meter (0.5mm). The cut-off was converted to cutoff frequency based on the sample frequency of the laser. In a similar way, a high pass filter was applied to obtain the microtexture data. The same cutoff was used since at that specific point is the separation between both wavelengths.

  The magnitude of the Frequency Response Function (FRF) of an nth order low-pass Butterworth filter is shown in equation (17).

$$|H_{LP}(jw)| = \frac{1}{\sqrt{1 + \left(\frac{w}{w_c}\right)^{2n}}} \qquad (4.1)$$

  w_c = Cut-off frequency

  In the same way, equation (18) represents a high-pass Butterworth filter.

$$|H_{HP}(jw)| = 1 - |H_{LP}(jw)|$$

$$= \frac{\sqrt{\left(\frac{w}{w_c}\right)^{2n} + 1} - 1}{\sqrt{\left(\frac{w}{w_c}\right)^{2n} + 1}} \qquad (4.2)$$

  Based on equations (4.1) and (4.2), figure (4.3) represents the normalized frequency response of each filter. At gain 0.707 (or -3 dB) it's the cutoff frequency of both filters. For the low pass filter, all the data before the cutoff frequency will pass through. The opposite occurs for the high pass filter.

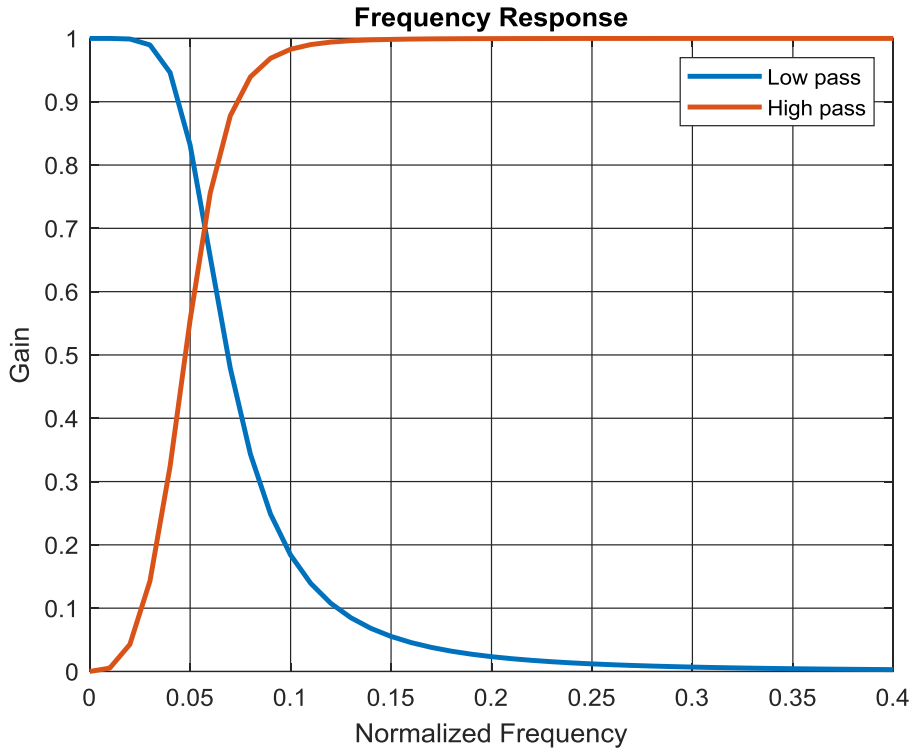

Figure 4-3 Raw data histogram

- A filter was applied on the raw data of each wavelength to eliminate remaining outliers on either end of the global distribution until 0.2% of the total data is removed. The 0.2% criteria was based on Walton's [51] results of spike errors when examining multiple raw texture data sets. [51] had a similar data resolution to this project, since he also used an LTS to collect data.
- MPD was computed using the specified ASTM E1845 standard [57].

Figure (4.4) and (4.5) represent one line of one scan (each scan has 100 lines), comparing the raw data and the data after the corresponding filter was applied. Figure (4.4) shows the

effect of a low pass filter. The filtered data follows the same path as the raw data, except in the peaks where the filter data is much smoother. Figure (4.5) shows the effect of a high pass filter; this means the data with the higher frequency.

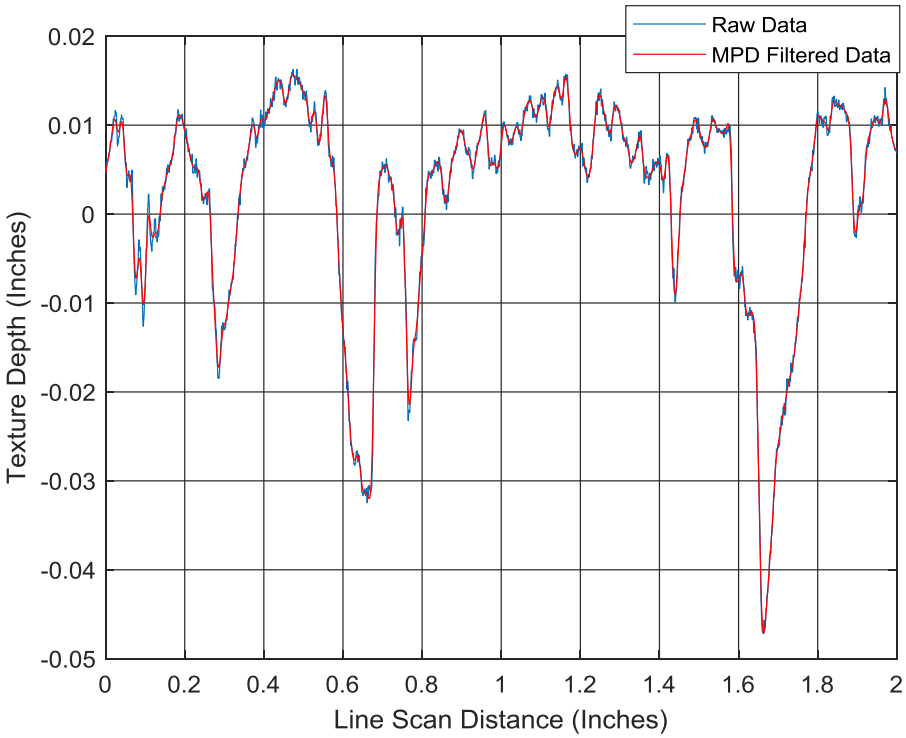

Figure 4-4 Low pass filter

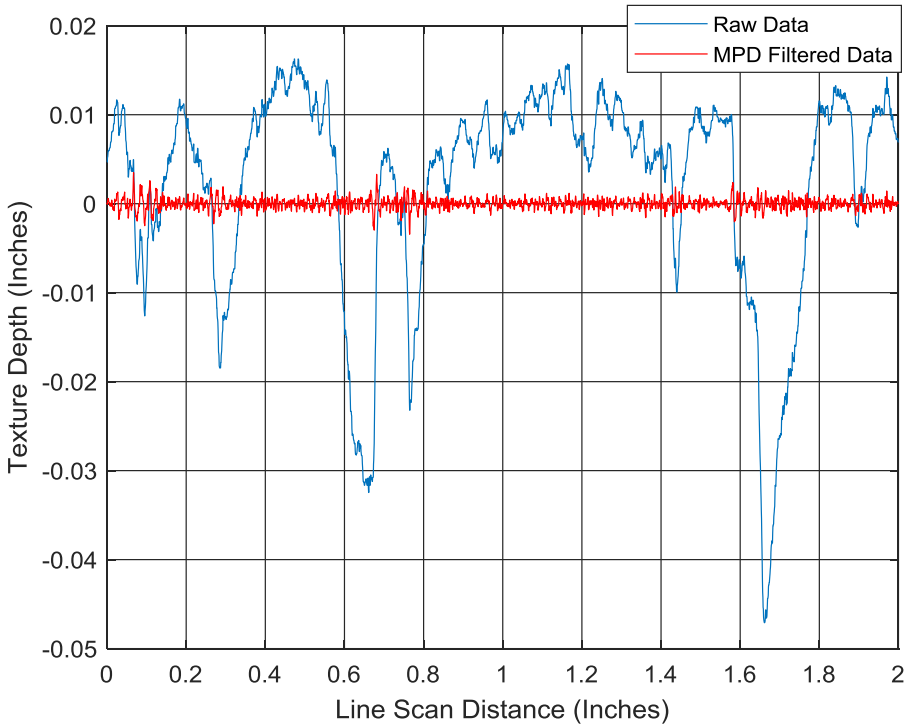

Figure 4-5 High pass filter

Before presenting the filtered data for each wavelength, it is essential to study the scanned raw data to see if there is any meaningful observation. Figure (4.7) shows the raw data of 3 scans in a three-dimensional representation from a top-view. The scale of colors is shown in figure (4.6). Red represents the top of the surface and as it reaches pink the surface is deeper with respect to the highest point in the surface. The 3 scans in figure (4.7) represent from left to right: a new road, 1.5-year-old road and 4-year-old road. The new road and 1.5-year-old scan were taken in the long leg, and both are affected by daily vehicle passengers and weather. On the other hand, the 4-year-old road scan was taken in an area of the curvature section where vehicles would normally not drive through, meaning that this scan is mainly affected by weather. By pure observation, the difference between the

condition of the three roads is visible; the 4-year-old road is more degraded and in a worst condition compared to the other two scans. Also, the new road scan is more uniform color (majority is yellow) than the 1.5-year-old road.

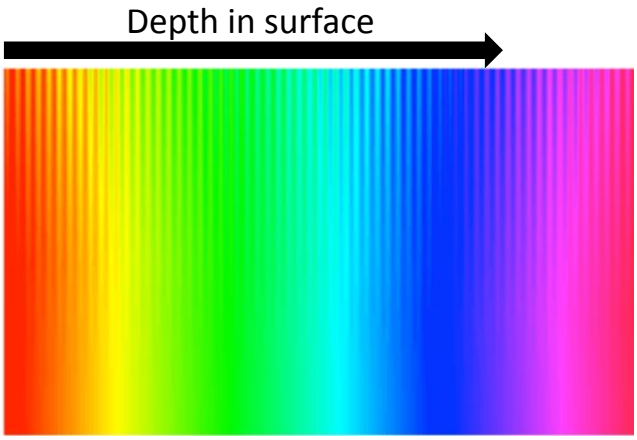

Figure 4-6 scale of color

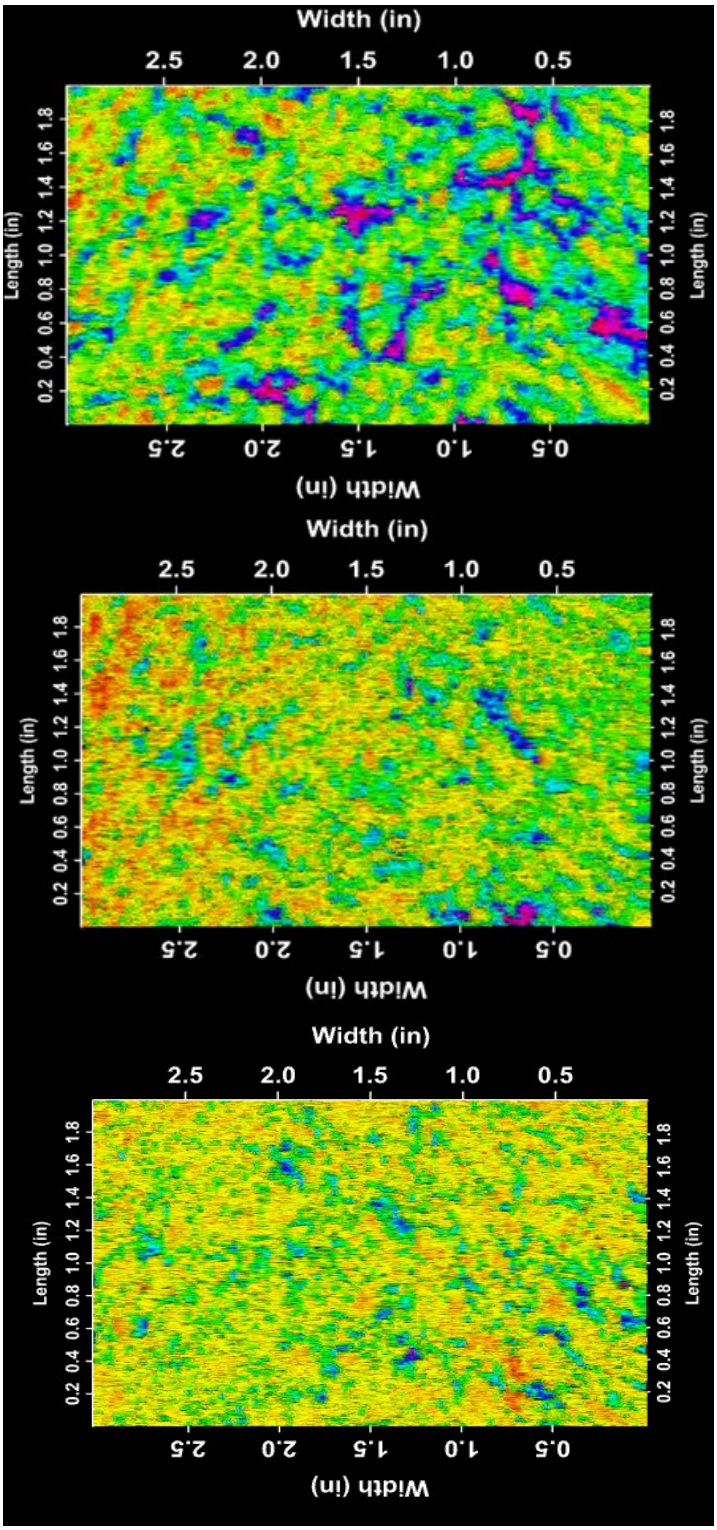

Figure 4-7 Raw data from top view

4.2.1 Before Repaving

First, the data before repaving the road is studied. It is assumed that there is not a major difference between the long and short leg and that both should have the same surface texture since historically they have been repaved at the same time. A quick plot is done to confirm this statement. Figures (4.8) and (4.9) represent the MPD values at each mile post before the road was paved for each wavelength. Each point represents the average value between the right and left side for each specific mile post. Both figures show that there is not a trend throughout the track, and the MPD magnitude is similar for both the long and short leg in each specific texture.

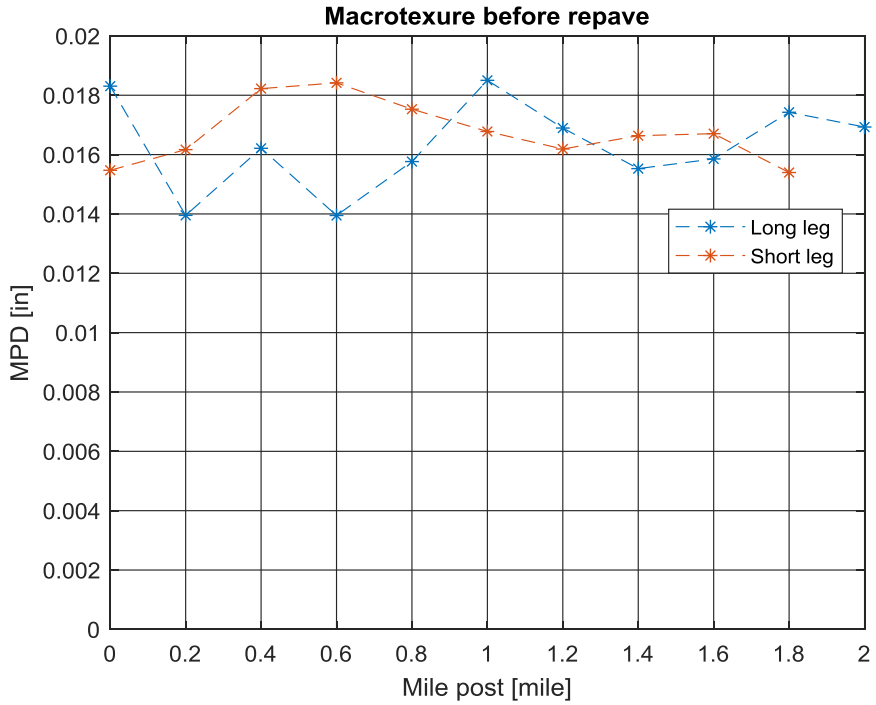

Figure 4-8 Macrotexture throughout the track

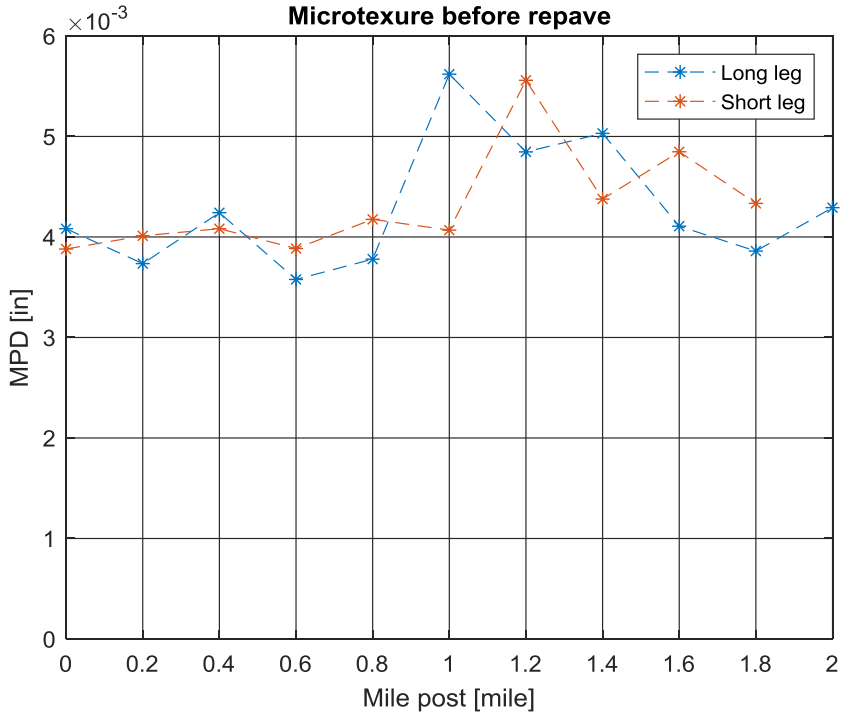

Figure 4-9 Microtexture throughout the track

As previously mentioned, the right and left side of the lane were affected by vehicle passengers, light trucks and weather. The comparison between those measurements and the center of the lane (which is only affected by weather) is represented in figures (4.10) and (4.11). The main idea is to perceive the difference in MPD from two areas in the same road, where one is affected by vehicle passengers and the other one is not. Each data point in figure (4.10) and (4.11) represents the average value of all the available data points of the specific reference. In both images, it is observed that the average MPD value smaller for the center lane. In addition, the impact of vehicle passengers affects more the road at the macrotexture level, since the difference between the center and right/left side is higher in the macrotexture level than micro.

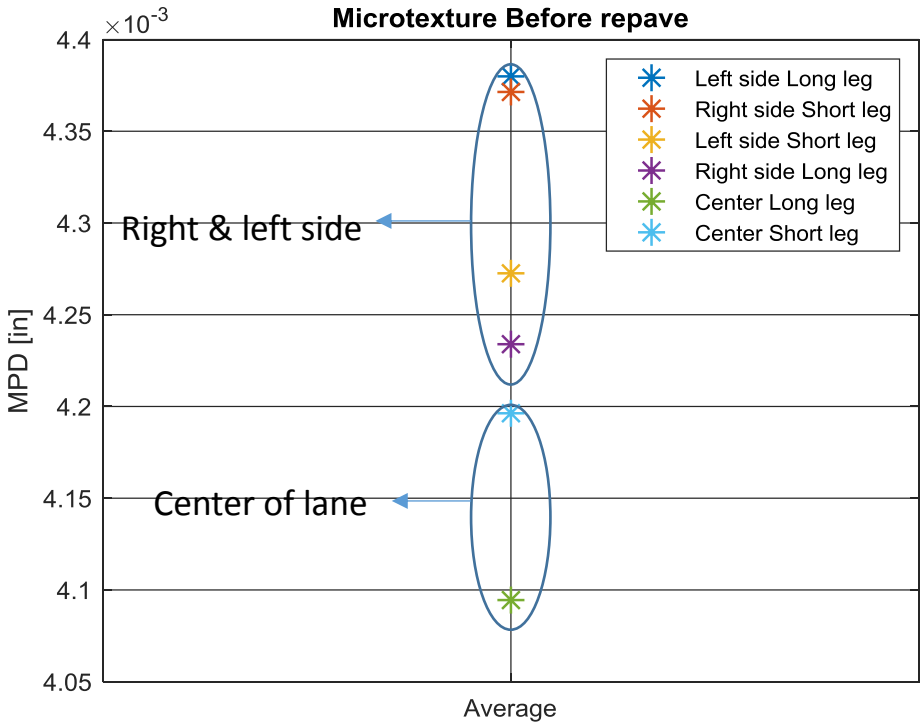

Figure 4-10 Microtexture before repaved

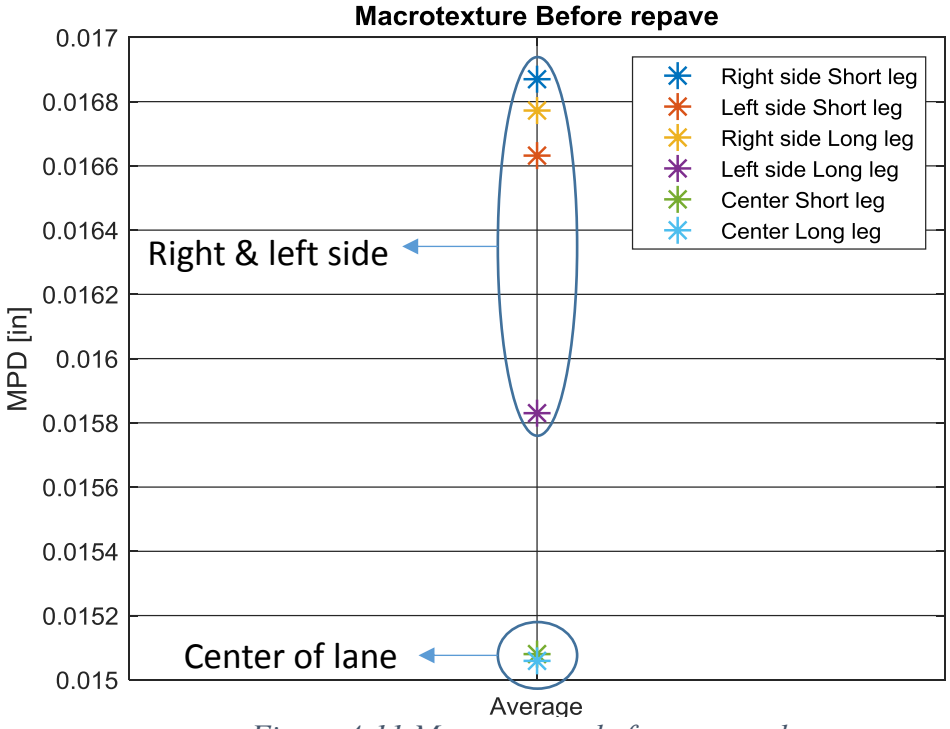

Figure 4-11 Macrotexture before repaved

Lastly in this section, figures (4.12) and (4.13) compare the previous data points with the 4-year-old road section to see how much impact does weather has in the long term. At the macrotexture level, the surface texture greatly degrades. The MPD increases approximately by a factor of 1.5, from a 1.5 to 4-year-old road. However, in the micro level, the weather effect does not seem to have an impact, the surface texture does not degrade much over time. The MPD value of the 4-year-old road is actually smaller than the MPD of the 1.5-year-old road.

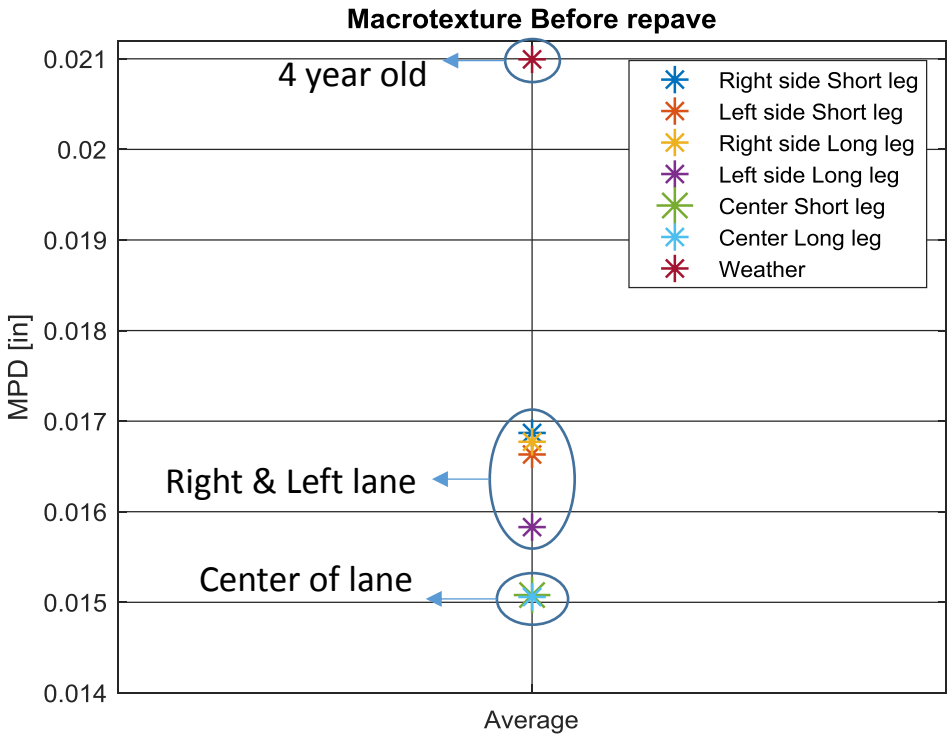

Figure 4-12 Macrotexture weather effect

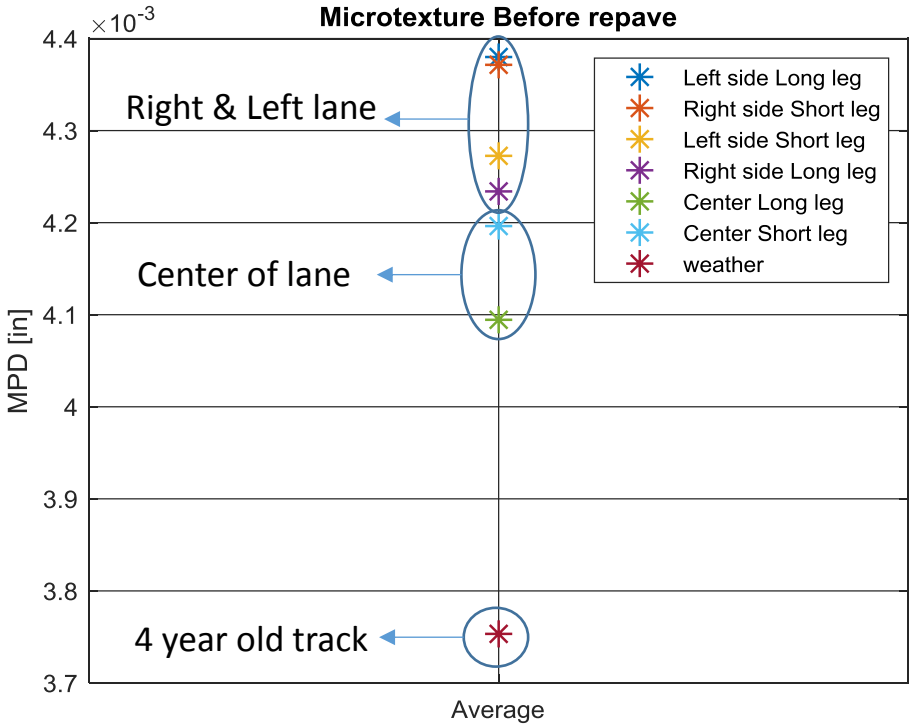

Figure 4-13 Microtexture weather effect

4.2.2 After Repave

After doing a general study of the data before repaved, it is possible to start analyzing the data after the road was repaved. The Arizona Proving Grounds was repaved at the end of April 2018. Then, some time was allowed before taking measurements for allowing the road to "break in". Based on a professional suggestion, 1-3 months after the road was repaved was suggested for taking the new measurements.

Just like before, figures (4.14) and (4.15) represent the MPD values throughout the track for each wavelength. As a reminder, there was a sandstorm while taking these

measurements in the long leg and not all the data was collected. Similar as before, there is not a noticeable pattern throughout the track. However, the magnitude of the values is perceptibly lower than in the previous section.

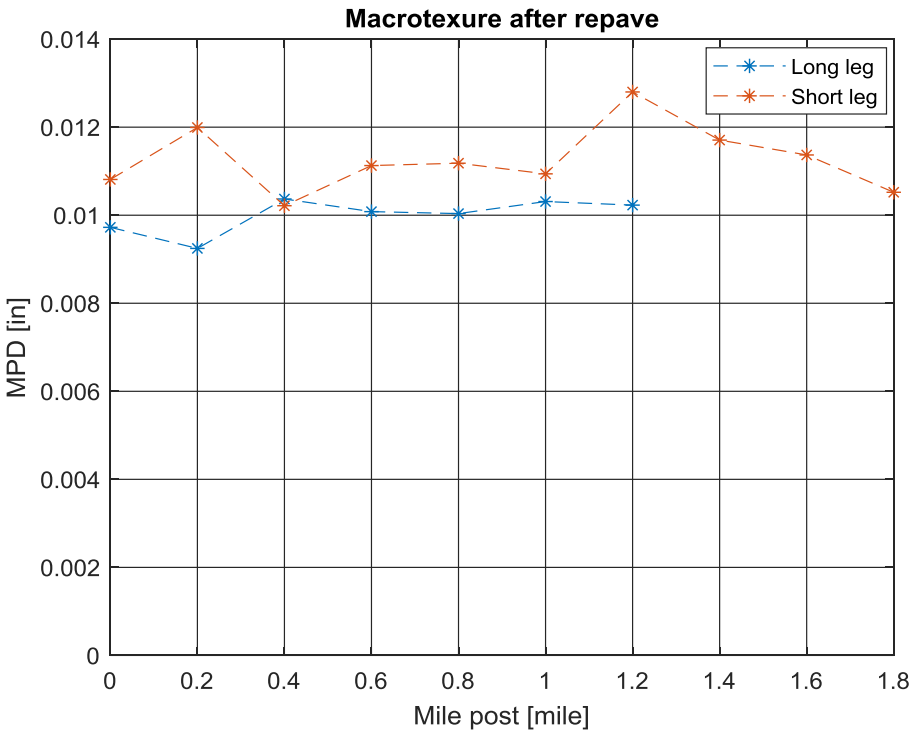

Figure 4-14 Macrotexture data throughout track after repaved

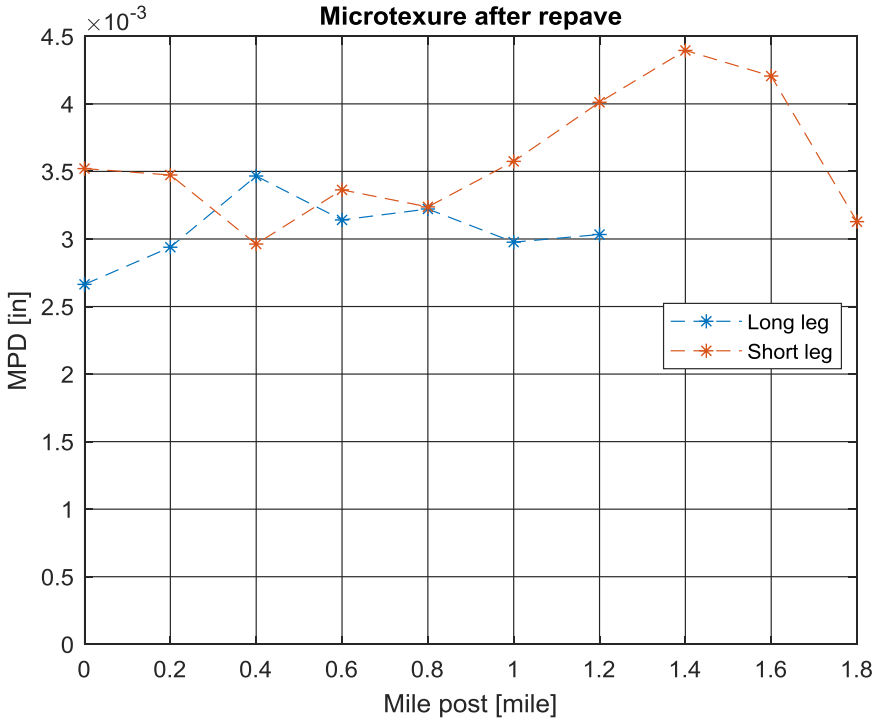

Figure 4-15 Microtexture data throughout track after repaved

One of the main objectives of this project was to quantify how much a road degraded in a span of 1.5-years from the perspective of micro- and macrotexture. Figures (4.17) and (4.16) represent the averaged MPD value for each section of the road before and after repaved. In both wavelengths, the MPD in the center of the lane is always less than the value of the right/left side. This is noticed even in the new road that only had 2-3 months of vehicles driving over. In addition, there is a substantial difference in MPD between the two sections. For the macrotexture wavelength, in average, there is a change of 36% in MPD between before and after repaved. This value was the average of only the data of the

right and left side from both legs, since the project is interested in learning how much the road degrades due to coast-down testing. On the other hand, the microtexture MPD changed approximately 23%.

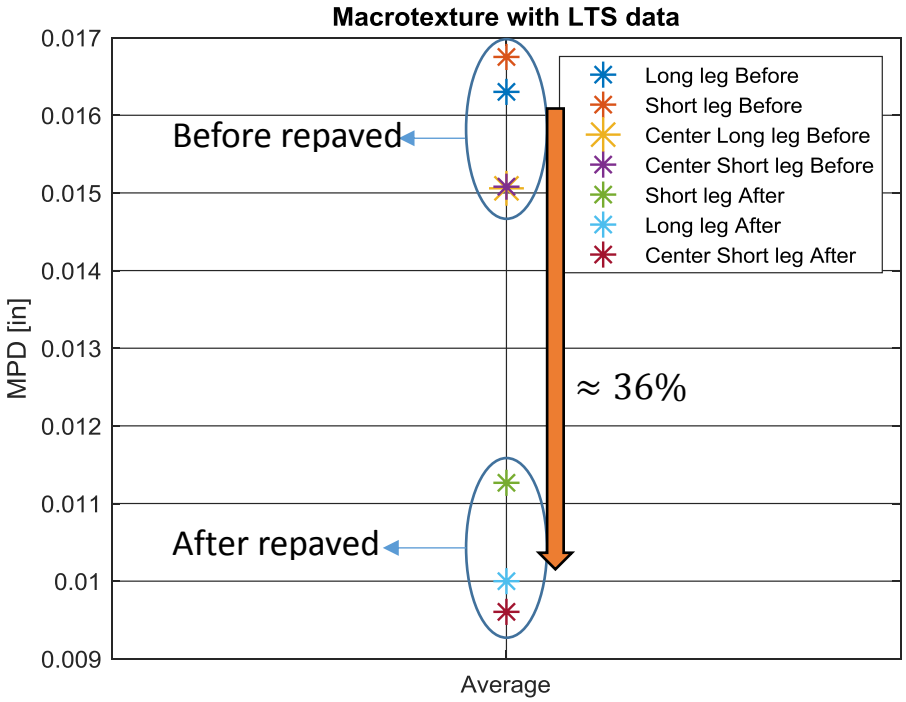

Figure 4-16 Macrotexture comparison

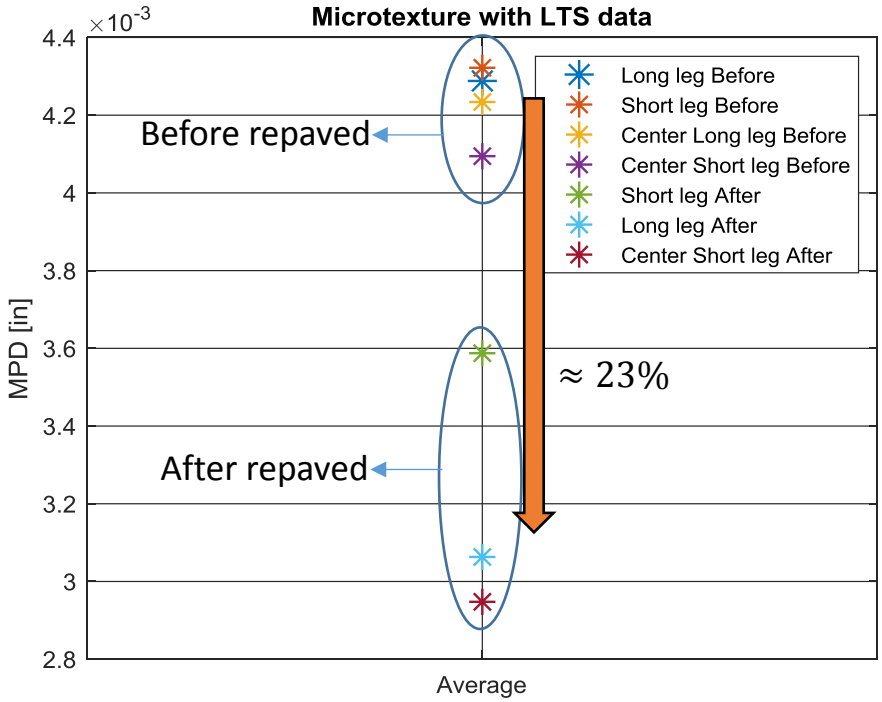

Figure 4-17 Microtexture comparison

Before arriving at any conclusion, it is necessary to study how the data is distributed. Figure (4.18) and (4.19) display the distribution of the data superimposed on a normal distribution curve. Also, table (5) contains statistical information to support the mentioned figures. In general, figure (4.19) shows that the data does not seem to follow a normal distribution for the microtexture wavelength. Figure (4.19) shows that the microtexture data looks skewed to the right. The range of the data after the road was repaved seems to be smaller in both wavelengths, inferring that the road surface is more uniform in that condition. As a result of the range being smaller after the road was repaved, the standard deviation (STD) follows the same pattern as shown in table (4.1). There was a decrease of 36% and 10% of STD for the macro- and microtexture, respectively.

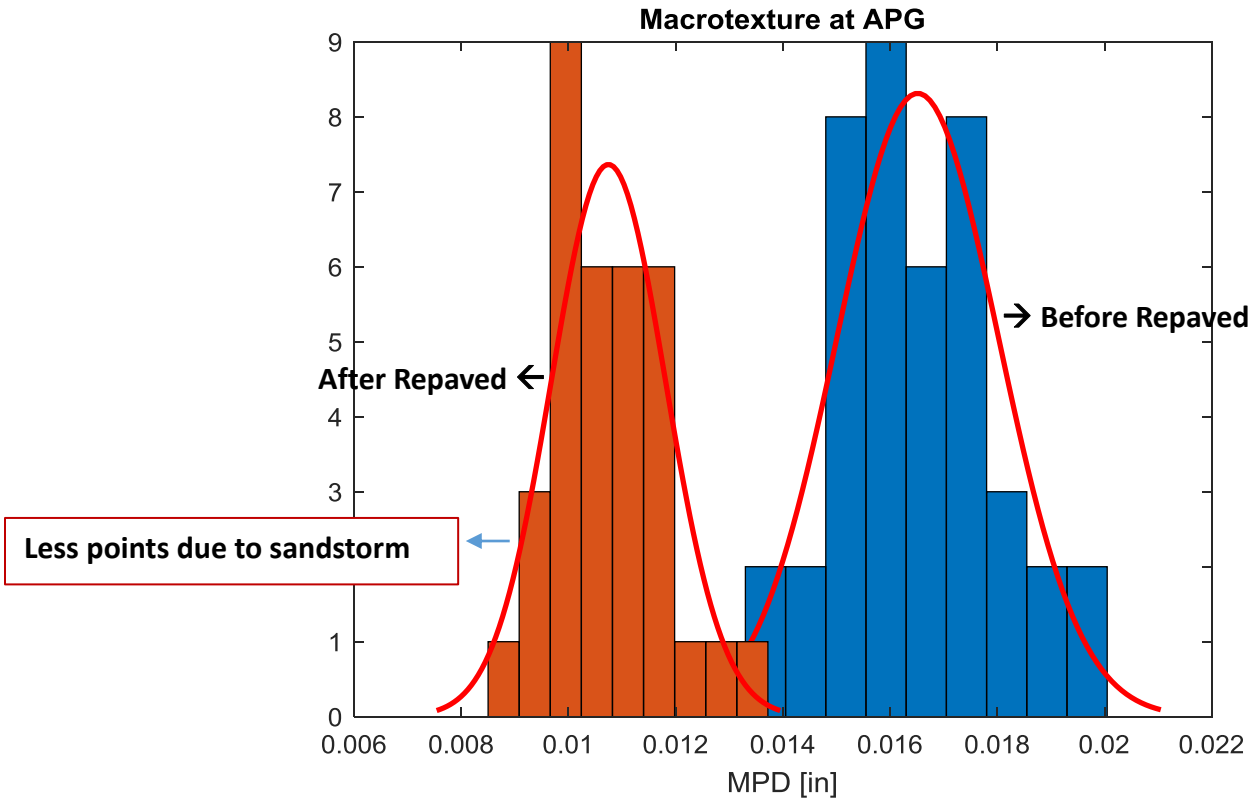

Figure 4-18 Normal distribution Macrotexture

Table 4-1 Normal distribution statistics Macrotexture

	Before Repave	After Repave
Mean	0.0165	0.0107
Standard Deviation	0.0015	0.0011

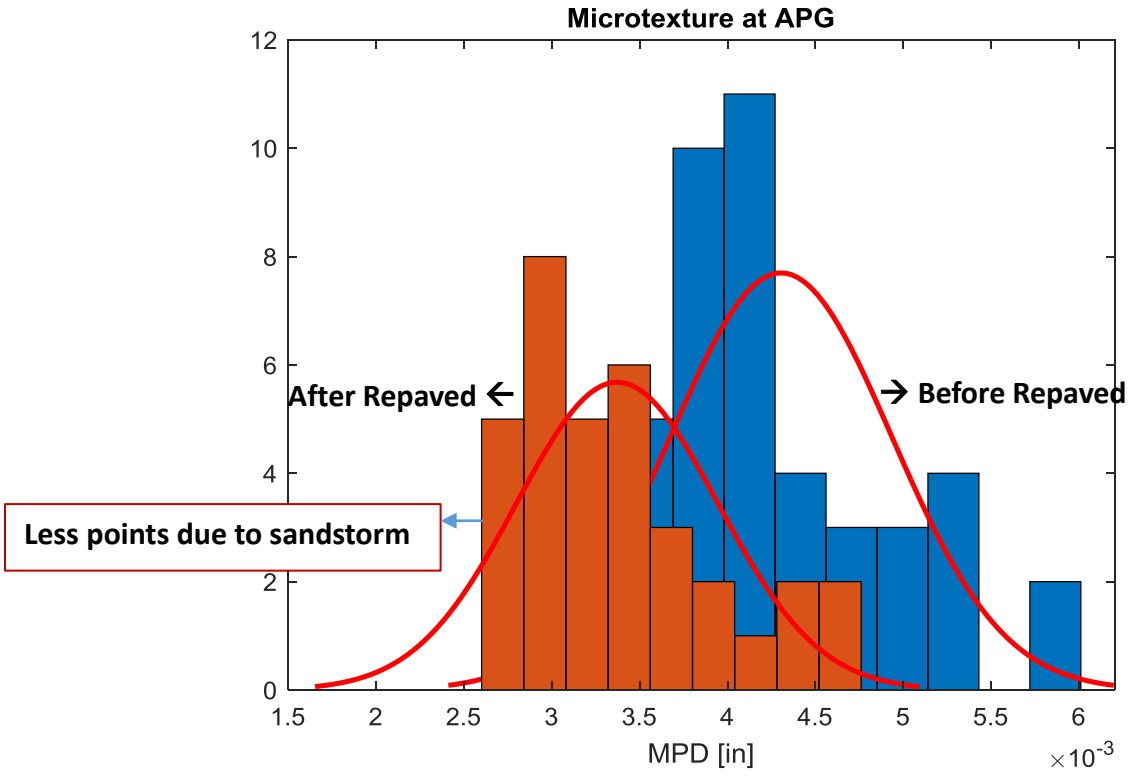

Figure 4-19 Normal distribution Microtexture

Table 4-2 Normal distribution statistics Microtexture

	Before Repave	After Repave
Mean	0.0043	0.0033
Standard Deviation	0.00063	0.00057

Figure (4.20) represents 4 different road surfaces with the same standard deviation. It is noticeable that the standard deviation is not the best parameter to fully characterize the roughness or texture of a surface. Instead, a frequency analysis could be more useful.

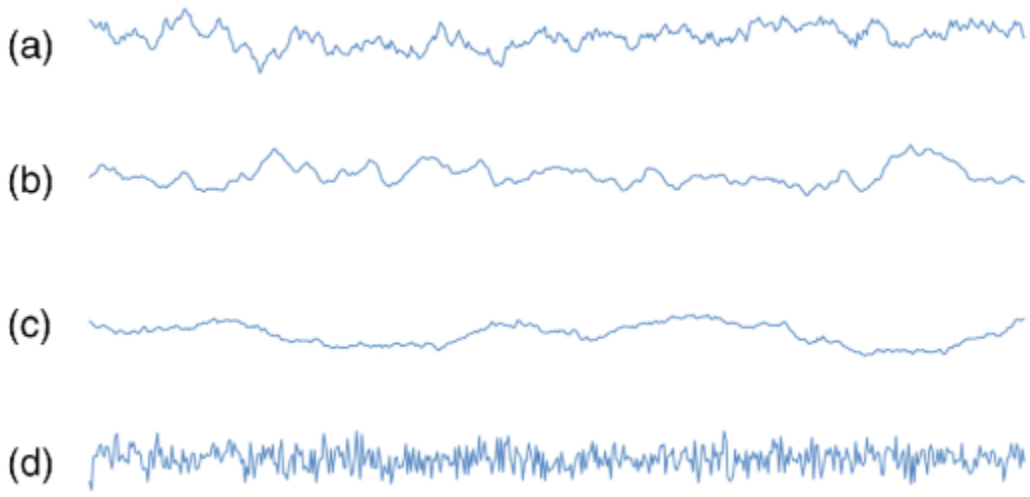

Figure 4-20 Road surfaces [60]

There are different methods available to characterize a random process and decompose it to obtain the required information. Some examples are: autocorrelation function, time evolution of the probability density/mass function, spectral density function, etc. Each method has its own advantages or disadvantages depending on what information the user is trying to obtain.

One of the most common ways of characterizing a random process is via a power spectral density (PSD). PSD is a type of frequency-domain analysis, which refers to the spectral power distribution that would be found per unit time [61]. In other words, it is the measure of signal's power content as a function of frequency. When a signal is displayed in the form of frequency spectrum, certain aspects of the signal or the underlying process producing it are revealed [62]. PSD has an extensive range of applications, from stochastic processes, physics and engineering.

PSD is a common mathematical tool use for analyzing surface roughness. In this specific application, a PSD plot allows a representation of the amplitude of a surface's texture as a function of the spatial frequency of the roughness [62]. Spatial frequency is the inverse of the wavelength of the roughness features. As a result, PSD function provides a graphic representation of how certain features are distributed along the surface, which otherwise could pass unnoticed. In addition, PSD plots representing surface roughness are usually plotted in log-log coordinates, because both axes vary over a wide range.

As previously mentioned, each scan taken by the LTS is composed of 100 lines. The PSD of one scan is the average of the PSD of each line. As a first step to study the characterization of the road surface, the idea is to compare the PSD of different lines

corresponding to the same scan. Figure (4.21) shows the PSD of 4 arbitrary lines in a scan. The 4 PSD profiles overlap with small observable differences, but in general they have the same trend and magnitude. Similar PSD profiles indicate that the quality of the scan was consistent and well maintained.

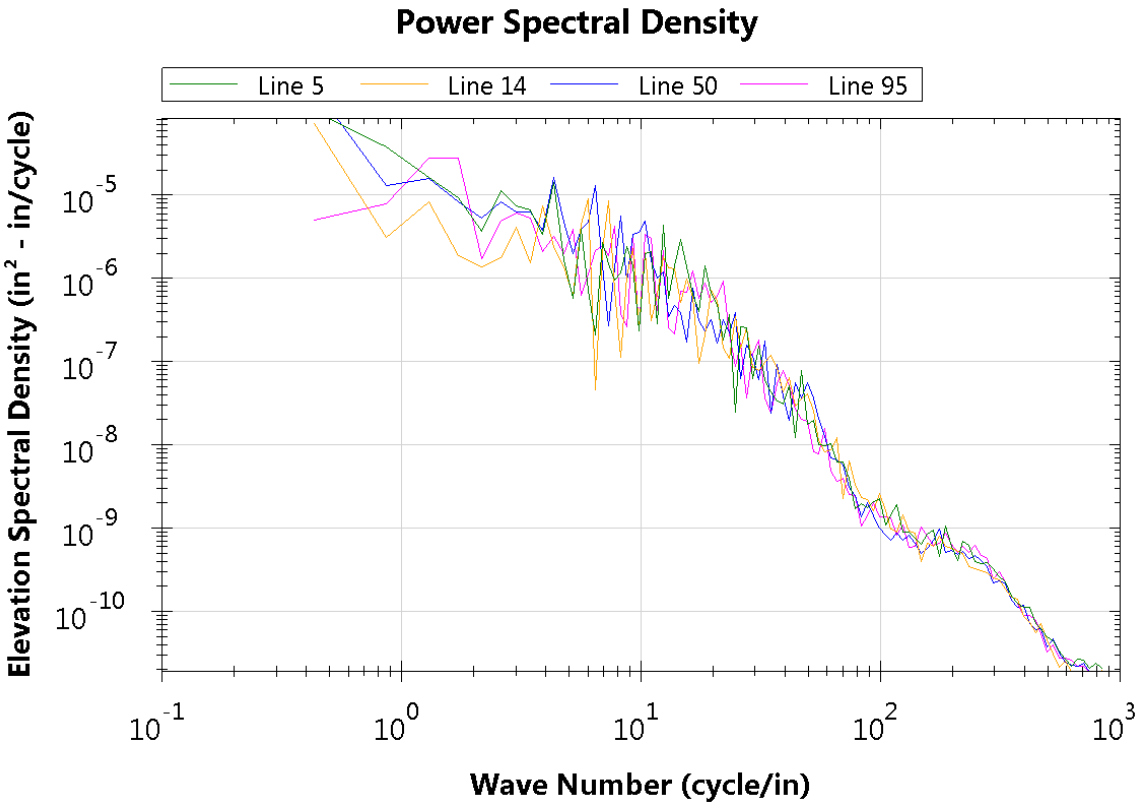

Figure 4-21 PSD comparison between lines

Then, figure (4.22) represents the PSD plot for the surface texture before and after repaved for two scans. Both scans where taken in the same spot of the proving grounds in Arizona. At a first glance, both curves have similar trends. In both cases, the curve as a whole has a

slope that goes downwards from left to right. This means, that the amplitude spectral density starts high for small wave numbers and it decreases as the wave number increases. This result is coherent because at small wave numbers, which corresponds to bigger wavelengths (high end of macrotexture), the variation of road surface's height is larger meaning that the waves have relatively high amplitudes. However, as the wave number increases (wavelengths decrease), the individual stone chips affecting the road surface have a relatively smaller amplitude. In addition, figure (4.22) has in general a linear trend which is characteristic of hard roads [63].

Even though both curves are comparable, it is noticeable that for the entire plot the amplitude of the post-repave PSD is always smaller than the pre-repave PSD. This indicates that in general the post-repave road is smoother than the pre-repave since it has smaller variations in road surface amplitude throughout each wavelength. In addition, the biggest difference in amplitude pre- and post-repave data is at smaller wave numbers (macrotexture wavelength). This explains why there was a larger percentage change in the MPD at the macrotexture level between before and after repaved.

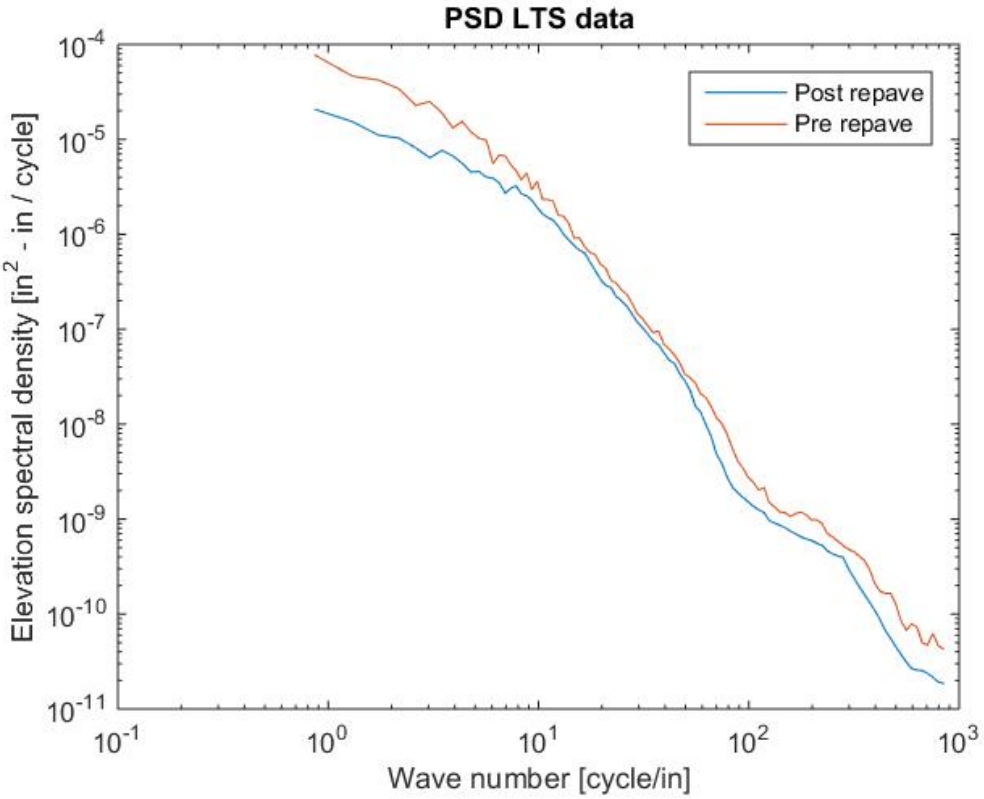

Figure 4-22 Power Spectral Density

In order to validate the results obtained by the laser texture scanner, it was important to compare them to another device. As previously mentioned, surface texture data from the same road was collected with a RoboTex device. The RoboTex is able to collect long strips of surface data, but its capability is limited to obtain only data at the macrotexture level.

Figure (4.23) represents the macrotexture data before and after repaved for both the RoboTex and LTS. In general, both devices calculated similar MPD values, and in both cases, there is a noticeable difference between the MPD before and after repaving. The

main difference between both devices is the MPD values after repaving. The RoboTex measured a higher surface roughness than the LTS. Table (4.3) shows the average MPD value for each device.

Nevertheless, other studies have compared the texture roughness obtained from different methods. Fisco [55] took measurements from distinctive surfaces with an LTS, Dynatest laser profiler, Circular Texture meter testing and Sand Patch testing. After analyzing the data, [55] obtained a small discrepancy between the MPD values from each method. Depending on the methodology, each one has its own possible sources of error, and at a macrotexture level a small error could make a noticeable difference. By comparing the error percentage range from couple of literature reviews [55] [64], it is possible to establish that the deviation in values between the LTS and RoboTex in this project is within an acceptable range.

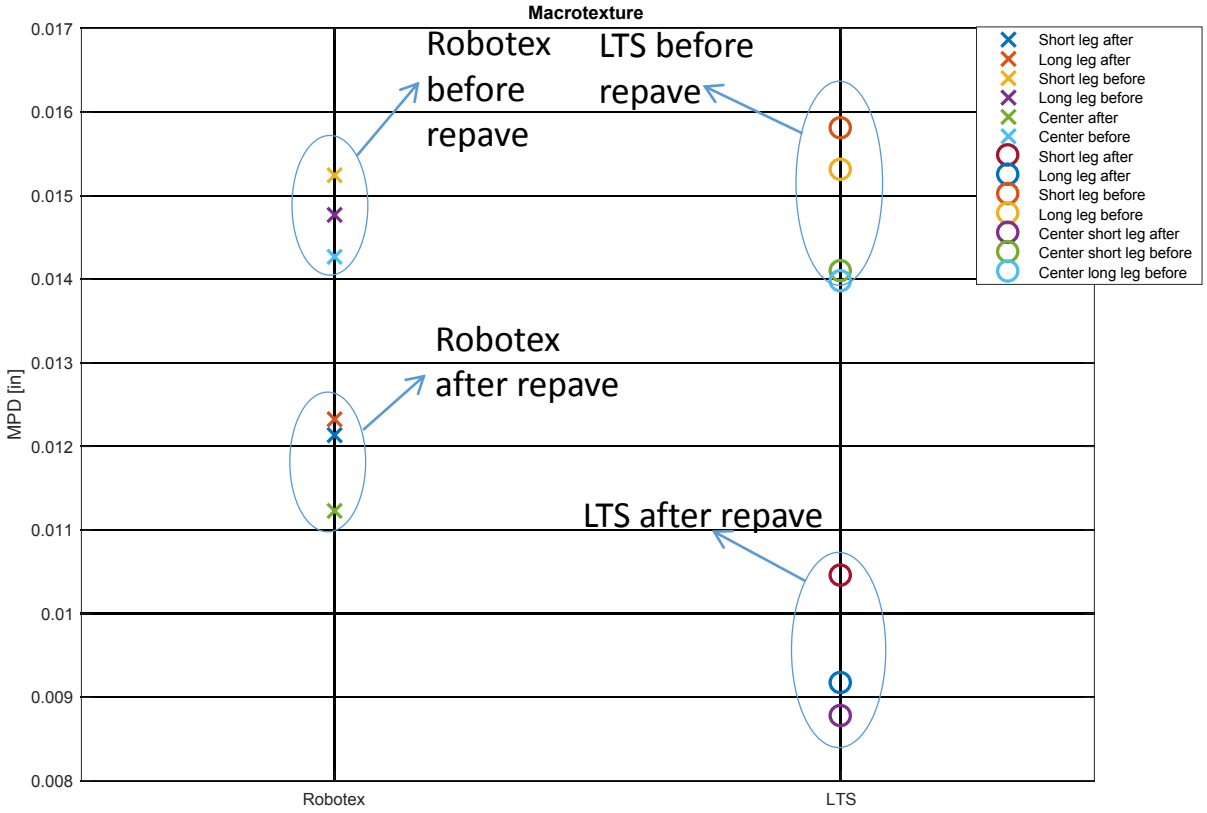

Figure 4-23 Comparing RoboTex vs LTS

Table 4-3 Average MPD RoboTex and LTS

	Laser Texture Scanner	RoboTex
MPD Before Repaved	0.0148	0.0148
MPD After Repaved	0.0095	0.0119

Finally, after analyzing, and validating the data obtained from the proving grounds, it is possible to derive a relation of how much a road degrades due to the effect of vehicles and weather. First, a linear degradation was assumed since the data available was collected only at two instances. Then, an average of the entire data set was done for each wavelength, (excluding points in the center of the lane). Figure (4.24) represents the linear degradation the road goes through in a span of 1.5 years for each wavelength. As expected, the slope of the microtexture data is much smaller than the macrotexture one. This degradation is also represented in equation (4.3) and (4.4) as a function of change in MPD per day.

Equation for microtexture degradation:

$$MPD_{micro} = 1.1215 * 10^{-6} * x + 0.001955 \qquad (4.3)$$

Equation for macrotexture degradation:

$$MPD_{macro} = 1.08411 * 10^{-5} * x + 0.00981 \qquad (4.4)$$

$$x = days$$

$$MPD\ is\ in\ inches$$

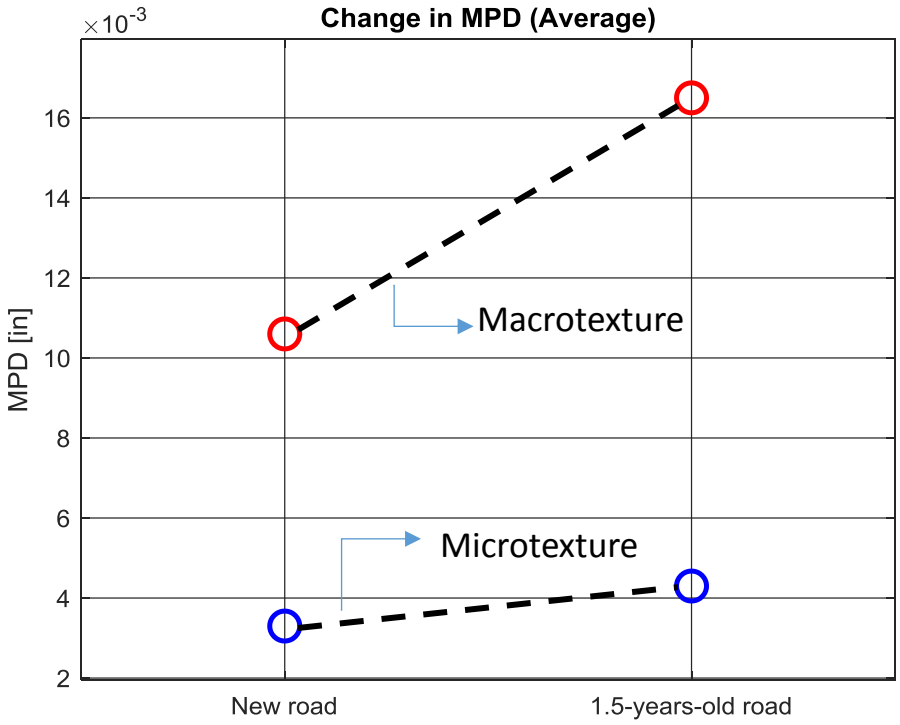

Figure 4-24 Road surface degradation

4.3 Conclusion

This chapter discussed the most important part of this thesis which is to study and quantify the change in surface texture for different wavelengths. First, the appearance of spike errors is relevant to all optical profilometers and should be taken into account. Then, based on the data, it seems that at small wavelengths data does not follow a normal distribution curve. Also, as previously mentioned, the center lane is divided in 3 sections -right, left and center of the lane. Results proved that the impact of the vehicle in the right/left side made a

significance difference in the road texture. The center of the lane's MPD was always lower compared to the sides of the lane. In addition, the 4-year-old road showed that weather mostly affects the macrotexture wavelength. Another important contribution of this chapter is the percentage degradation of road surface. For the specific type of road in the Arizona proving ground, the road degraded 36% and 23% for macro- and microtexture wavelengths in a span of 1.5 years, respectively. These analysis lead to a mathematical representation of road surface degradation per day for each wavelength (assuming a linear degradation). In conclusion, there is a clear difference in road surface texture between a new road and a road used for daily coast-down tests, which could potentially be affecting the results of the coast-downs.

Chapter 5 : Conclusion and Future Work

5.1 Summary and Conclusion

Fuel consumption along with emissions and vehicle performance are crucial elements in the development of new vehicles. Automotive companies are putting significant effort in testing and measuring more accurately these parameters. Specifically, fuel consumption can be measure by doing a coast-down test or by measuring aerodynamic drag, rolling resistance and parasitic separately in a lab. For both options, it is important to capture or model all of the parameters affecting a vehicle. This thesis provided a detailed description of what parameters affect rolling resistance with an emphasis on road surface texture. The main objective was to study how much does a road, where coast-down tests take place, degrades over time with respect to the micro- and macrotexture wavelengths.

For this project, multiple measurements were taken in a proving ground in Arizona where vehicles are constantly doing coast-down tests. Measurements were collected before and after the road was repaved with an optical profilometer. From the raw data, it was possible to observe noticeable differences between the old and new road. Then, it was possible to study the degradation of each wavelength after applying the corresponding filters to the

data. There was a clear difference in surface texture between the section where vehicles drove over, and the center of the lane were vehicles were not supposed to drive over. Also, it was observed how macrotexture wavelength is greatly impacted by weather effect in the long term. On the other hand, microtexture did not seem to degrade just by weather effect.

Based on the results, macrotexture is more sensitive than microtexture to weather and vehicles impact. Both wavelengths degraded over time but macrotexture had a higher degradation rate. It can be concluded that macrotexture has a bigger impact on rolling resistance. Then, by assuming a linear degradation it was also possible to develop a mathematical model representing the degradation of road surface per day. It is important to note that non-heavy vehicles transited this specific road, as a result, there was a smaller impact on the road compared to the case with heavy vehicles.

Automakers repaved roads where they test vehicles every couple of years; there is not a standard of how often they should repave, so automakers do it based on their own judgement. When coast-down tests are performed, the impact of the road on the vehicle is assumed to be a constant parameter. However, if the road is degrading over time, its surface texture would be getting rougher and that would increase rolling resistance and fuel consumption of a vehicle. It is important to include road surface texture as a parameter affecting the losses in rolling resistance to avoid measuring a wrong fuel consumption. With the high competition between automakers, ± 1 MPG in a vehicle makes a difference in automobile performance, marketing, sales, etc.

5.2 Future Work

Although chapter 4 provides an initial linear model to represent road surface degradation, further experiments need to be conducted. One key experiment would be to collect data when the road is approximately 1-year-old, or after 2 years if the road has not been repaved. This would allow a better representation of the road degradation since currently it is assumed to be linear. Additionally, this thesis focused on micro- and macrotexture wavelengths, however, literature review suggests that it would also be valuable to study the effect of road surface degradation at the largest wavelength, such as unevenness.

Experimental tests between different road materials would give a deeper sense of how different roads change over time. Nowadays it is more common to add an aggregate to the composite material. Aggregates have a significant impact on the durability, strength, weight and shrinkage of composite materials. Depending on the type of aggregate, it could slow the road surface degradation. In the last couple of years, the Arizona proving grounds acquired a high-quality aggregate compared to the previous one. This suggests, that if the new aggregate had not been used, there would have been a higher road surface degradation between before and after repaved.

Furthermore, this thesis focused mainly on rolling resistance, but other parameters should also be studied. For example, in aerodynamic drag one key element is what type of wind tunnel is being used. Drag coefficient will vary depending if it is a static or moving wind tunnel, and different equations may need to be implemented to compensate for different factors. Even if it is a moving wind tunnel, there are different types -1 belt, 3 belts, or 5

belts. On the other hand, there is not a standardized process of how to measure parasitic losses. It would be interesting to compare the different methodologies that companies or research centers implement. In addition, it would be beneficial to study the parasitic losses of the different types of hybrid vehicles (in series, parallel, combine, etc.). In general, it is important to analyze each factor in order to improve the overall quality of road load and get more accurate results.

References

[1] E. P. Agency, "Federal Register," 23 09 2010. [Online]. Available: https://www.epa.gov/fueleconomy/history-fuel-economy-labeling.

[2] R. Rapier, "Oil Price," 24 10 2013. [Online]. Available: https://oilprice.com/Energy/Crude-Oil/How-the-1973-Oil-Embargo-Still-Affects-the-US-Energy-Agenda-Today.html.

[3] U. o. C. Scientists, "ucsusa," March 2011. [Online]. Available: https://www.ucsusa.org/sites/default/files/legacy/assets/documents/clean_vehicles/UCS-The-National-Program.pdf.

[4] Union of Concerned Scientists, "ucsusa," 6 December 2017. [Online]. Available: https://www.ucsusa.org/clean-vehicles/fuel-efficiency/fuel-economy-basics.html#.XDYohlVKjA4.

[5] J. Halpert, "What if US fuel economy standards went away?," Ensia, 2018. [Online] Available: https://medium.com/ensia/what-if-u-s-fuel-economy-standards-went-away-254fb8b1500e

[6] N. Carey, "Reuters," 29 March 2018. [Online]. Available: https://www.reuters.com/article/us-autoshow-new-york-suvs/lured-by-rising-suv-sales-automakers-flood-market-with-models-idUSKBN1H50KI.

[7] G. Rizzoni, "The Conversation," 28 September 2018. [Online]. Available: http://theconversation.com/freezing-fuel-economy-standards-will-slow-innovation-and-make-us-auto-companies-less-competitive-102701.

[8] European Automobile Manufacturers Association, "ACEA," 12 April 2018. [Online]. Available: https://www.acea.be/publications/article/overview-of-incentives-for-buying-electric-vehicles.

[9] Z. Shahan, "Clean Technica," 2 May 2018. [Online]. Available: https://cleantechnica.com/2018/05/02/new-swedish-car-policies-expected-to-spike-electric-vehicle-market-share-in-sweden/.

[10] K. Dowd and E. Hartman, "NCSL," 27 September 2017. [Online]. Available: http://www.ncsl.org/research/energy/state-electric-vehicle-incentives-state-chart.aspx.

[11] B. Palmer, "NRDC," 28 August 2018. [Online]. Available: https://www.nrdc.org/stories/fuel-efficiency-standards-dont-just-help-curb-climate-change-they-also-create-jobs.

[12] G. Rizzoni, *ME7384 Lecture 2 Vehicle Road Load,* 2017.

[13] G. Kadijk, "TNO," 29 October 2012. [Online]. Available: https://www.transportenvironment.org/sites/te/files/publications/Road%20load%20determination%20of%20passenger%20cars%20-%20TNO-060-DTM-2012-02014.pdf.

[14] S. o. A. Engineers, "Road Load Measurement Using Onboard Anemometry and Coastdown Techniques," Standard J2263_200812, 2008.

[15] J. Hirsch, "The Seattle Times," 2 November 2012. [Online]. Available: https://www.seattletimes.com/business/hyundai-kia-inflated-fuel-economy-claims-on-900000-cars-epa-says/.

[16] D. Shepardson, "Reuters," 13 May 2016. [Online]. Available: https://www.reuters.com/article/us-generalmotors-suvs-idUSKCN0Y42CI.

[17] G. Le Good, J. Howell, M. Passmore and K. Garry, "On-Road Aerodynamic Drag Measurements Compared with Wind Tunnel Data," SAE Technical Paper 950627, 1995.

[18] J. Howell, C. Sherwin, M. Passmore and G. Le Good, "Aerodynamic Drag of a Compact SUV asMeasured On-Road and in the Wind Tunnel," SAE technical paper 2002-01-0529, 2002.

[19] H. Korst, R. White and D. Metz, "Road Evaluation of the Aerodynamic Characteristics of Heavy Trucks," SAE technical paper 2007-01-4297, 2007.

[20] A. Altinisik, "Aerodynamic coastdown analysis of a passenger car for various configurations," *International Journal of Automotive Technology,* vol. 18, no. 2, p. 245, 2017.

[21] F. Buckley, " ABCD - An Improved Coast Down Test and Analysis Method," SAE technical paper 950626, 1995.

[22] Mavuri, S, 2009, *Aerodynamic analysis of vehicle wheel-housings*, Doctor of Philosophy (PhD), Aerospace, Mechanical and Manufacturing Engineering, RMIT University.

[23] F. Buscariolo and A. Mariani, "Analysis of different types of wind tunnel's ground configuration using numerical simulation," SAE technical paper 2010-36-0078, 2010.

[24] G. Le Good, J. Howell, M. Passmore and A. Cogotti, "A Comparison of On-Road Aerodynamic Drag Measurements with Wind Tunnel Data from Pininfarina and MIRA," SAE technical paper 980394, 1998.

[25] D. Sahini, 2004, *Wind tunnel blockage corrections: a computational study,* Master of Science*,* Mechanical Engineering, Texas Tech University, Lubbock.

[26] H. Iwase, S. Yamada and H. Koga, "A New Approach to Measuring Road Load by Chassis Dynamometer and Wind Tunnel Tests," SAE technical paper 820377, 1982.

[27] J. Walter, D. Pruess and G. Romberg, "Coastdown/Wind Tunnel Drag Correlation and Uncertainty Analysis," SAE technical paper 2001-01-0630, 2001.

[28] S. Singh, N. Jadhav, P. Vishe and K. Gopalakrishna, "Methodology for Measurement of Inherent Driveline Frictional Force for a Vehicle in Coasting Mode," SAE International (2009-01-0416), 2009.

[29] B. Dayman, "Tire Rolling Resistance Measurements From Coast-Down Tests," SAE technical paper 760153, 1976.

[30] M. Passmore and E. Jenkins, "Measuring vehicle drag forces using an on-board microcomputer," Journal of Automobile Engineering, Volume 204, Issue 2, page 77-82, 1990.

[31] M. Passmore and G. Le Good, "A detailed drag study using the coast-down method," SAE technical paper 940420, 1994.

[32] Michelin, "The tyre - Rolling resistance and fuel savings," Societe de Technologie Michelin, 2003.

[33] D. Fuller, G. Hall and F. Conant, "Effect of Testing Conditions on Rolling Resistance of Automobile Tires," SAE Technical paper 840068, 1984.

[34] R. Karlsson, U. Hammarstrom, H. Sorensen and O. Eriksson, "www.vti.se/publications," 2011. [Online]. Available:

https://pdfs.semanticscholar.org/e249/d09809ddb88685c7c965b4d742a69e5c7b0d.pdf.

[35] D. Mukherjee, "Effect of Pavement Conditions on Rolling Resistance," American Journal of Engineering Research, Volume 3, Issue 7, page 141-148, 2014.

[36] P. Grover, "Modeling of Rolling Resistance Test Data," SAE technical paper 980251, 1998.

[37] Ejsmont, J., Taryma, S., Ronowski, G. et al. Int.J Automot. Technol. (2018) 19: 45. https://doi.org/10.1007/s12239-018-0005-4

[38] ISO-13473-5, "Characterization of pavement texture by use of surface profiles," ISO, 2009.

[39] U. Sandberg and J. Ejsmont, "Tyre Road Noise Reference Book," INFORMEX HB, 2002.

[40] X. Qiu, "Full Two-Dimensional Model for Rolling Resistance. II: Viscoelastic Cylinders on Rigid Ground," *Journal of Engineering Mechanics,* Volume 135, Issue 1, 2009.

[41] A. El Gendy and A. Shalaby, "Mean Profile Depth of Pavement Surface Macrotexture Using Photometric Stereo Techniques," *Journal of Transportation Engineering,* vol. 133, no. 7, 2007.

[42] Z. Li, Transportation Asset Management: Methodology and Applications, CRC Press, 2018.

[43] ASTM-E1926-08, "Standard Practice for Computing International Roughness Index of Roads from Longitudinal Profile Measurements," ASTM International, West Conshohocken, PA, 2015.

[44] "Pavement Interactive," [Online]. Available: https://www.pavementinteractive.org/reference-desk/pavement-management/pavement-evaluation/roughness/. [Accessed 14 February 2019].

[45] Laganier, R. and Lucas, J., "The Influence of Pavement Evenness and Macrotexture on Fuel Consumption," *Surface Characteristics of Roadways: International Research and Technologies*, STP1031-EB, Meyer, W. and Reichert, J., Ed., ASTM International, West Conshohocken, PA, 1990, pp. 454-459, https://doi.org/10.1520/STP23381S

[46] U. Sandberg and A. Bergiers, "Road surface influence on tyre/road rolling resistance," Report MIRIAM_SP1_04, December 31, 2011, Accessed on March 20, 2019. [Online] Available: http://www.miriam co2.net/Publications/MIRIAM_SP1_Road-Surf-Infl_Report%20111231.pdf

[47] J. J. Drugge and A. S. Trigell, "Studying Road Roughness Effect on Rolling Resistance Using Brush Tyre Model and Self-Affine Fractal Surfaces," in *The*

Dynamics of Vehicles on Roads and Tracks, - Proceedings of the 24th Symposium of the International Association for Vehicle System Dynamics, 2015, pp 273-280.

[48] U. Sandberg, "Rolling Resistance – Basic Information and State-of-the-Art on Measurement methods," Report MIRIAM_SP1_01, June 01, 2011, Accessed on March 20, 2019. [Online] Available: http://www.miriam-co2.net/Publications/MIRIAM_SoA_Report_Final_110601.pdf

[49] ASTM-E965, "Standard Test Method for Measuring Pavement Macrotexture Depth Using a Volumetric Technique," *ASTM,* 2015.

[50] A. Serigos, P. Buddhavarapu, G. Gorman, F. Hong and J. Prozzi, "The Contribution of Micro- and Macro-texture to the Skid Resistance of Flexible Pavement," Texas A&M Transportation Institute, Austin, Report SWUTC/16/600451-00085-1, Feb 2016. [Online] Available: https://static.tti.tamu.edu/swutc.tamu.edu/publications/technicalreports/600451-00085-1.pdf

[51] R. Walton, 2018, *Characterization of Road Surfaces Using High Resolution 3D Surface Scans to Develop Parameters for Predicting Tire-Surface Friction*, Master of Science, Mechanical Engineering, The Ohio State University, Columbus, Ohio.

[52] "Zygo," [Online]. Available: https://www.zygo.com/?/met/profilers/opticalprofilersabout.htm. [Accessed 14 February 2019].

[53] *Ames Engineering Laser Texture Scanner -User Manual.* [Manual]. United States: Ames Engineering, 2010.

[54] J. Jewett, H. Abe, S. Kameyama, A. Tamai, A. Kasahara and K. Saito, 2000, "Determination of the International Friction Index (IFI) using the Circular Texture Meter (CTM) and the Dynamic Friction Tester (DFT)," in SURF 2000: Fourth International Symposium on Pavement Surface Characteristics on Roads and Airfields, World Road Association- PIARC, Nantes, France.

[55] N. Fisco, 2009, *Comparison of Macrotexture Measurement Methods*, Masters of Science, Civil Engineering, The Ohio State University, Columbus, Ohio.

[56] "The Transtec Group," 28 February 2013. [Online]. Available: http://www.thetranstecgroup.com/pavement-engineers-release-updated-robotic-pavement-texture-profiler/. [Accessed 14 February 2019].

[57] ASTM-E1845, "Standard Practice for Calculating Pavement Macrotexture Mean Profile Depth," *ASTM,* 2015.

[58] P. Podulka, P. Pawlus, P. Dobrzanski and A. Lenart, "Spikes removal in surface measurement," in *14th International Conference on Metrology and Properties of Engineering Surfaces*, 2014.

[59] S. Katicha, D. Mogrovejo, G. Flintsch and E. de Leon Izeppi, "Adaptive Spike Removal Method for High Speed Pavement Macrotexture Measurements by Controlling the False Discovery Rate," *Journal of the Transportation Research Board,* vol. 2525, pp. 100-110, 2015.

[60] C. Mack, "SPIE digital library," 7 August 2018. [Online]. Available: https://www.spiedigitallibrary.org/journals/Journal-of-MicroNanolithography-MEMS-and-MOEMS/volume-17/issue-04/041006/Reducing-roughness-in-extreme-ultraviolet-lithography/10.1117/1.JMM.17.4.041006.full?SSO=1. [Accessed 18 February 2019].

[61] "Spectral density," Wikipedia, The Free Encyclopedia, 23 January 2019. [Online]. Available: https://en.wikipedia.org/w/index.php?title=Special:CiteThisPage&page=Spectral_density&id=879839733. [Accessed 15 February 2019].

[62] "Nanophys," Bruker Corporation, [Online]. Available: http://www.nanophys.kth.se/nanophys/facilities/nfl/afm/icon/bruker-help/Content/SoftwareGuide/Offline/AnalysisFunct/PowerSpectralDens.htm. [Accessed 15 February 2019].

[63] A. Brickman, J. Wambold and J. Zimmerman, "An Amplitude-Frequency Description of Road Roughness," pp. 53-67, 1971.

[64] Sezen, Halil & Fisco, Nicholas. (2013). "Evaluation and comparison of surface macrotexture and friction measurement methods." Journal of Civil Engineering and Management. Volume 19, pages 387-399, doi: 10.3846/13923730.2012.746237.

[65] "ICCT," April 2018. [Online]. Available: https://www.theicct.org/sites/default/files/CAFE_mpg_cars_Apr2018.png.

[66] DieselNet, "Emission Test Cycles". [Online] Available: https://www.dieselnet.com/standards/cycles/ftp75.php

[67] J. Wong, "Theory of Ground Vehicles," John Wiley & Sons, Inc, 2001.